

Bachelor's Thesis

Studien zur Messung der Top Quark Masse im dileptonischen Kanal am ATLAS Experiment

Studies on the Measurement of the Top Quark Mass in the Dileptonic Channel at the ATLAS Experiment

prepared by

Dominik Müller

from Wolfsburg

at the II. Institute of Physics

Thesis Period: 3rd April 2012 until 10th July 2012

Thesis Number: II. Physik-UniGö-BSc-2012/03

Supervisor: Dr. Kevin Kröniger
Dipl. Phys. Tamara Vazquez Schröder

First Referee: Prof. Dr. Arnulf Quadt

Second Referee: Prof. Dr. Ariane Frey

Abstract

The neutrino weighting algorithm can be used to extract a top mass measurement from events with a dileptonic $t\bar{t}$ decay. This thesis presents studies on this decay that are needed to reconstruct the event by using the neutrino weighting algorithm. Monte Carlo samples for 13 different top masses are used to study the neutrino pseudorapidity distribution on parton and reconstruction level.

It is shown that the neutrino pseudorapidity distribution can be sufficiently well described by a Gaussian distribution and a parameterization for the standard deviation of this distribution as a function of the top mass is obtained. A systematic deviation between data and fit, which indicates that the neutrino pseudorapidity distribution has two peaks, is discussed. Furthermore, the effects of the event selection are studied in a cutflow analysis.

In a last step, the missing energy resolution is studied and also parameterized as a function of the top mass.

Zusammenfassung

Im Rahmen dieser Bachelorarbeit werden Studien zum dileptonischen Zerfallskanal vorgestellt, die erforderlich sind, um diese Ereignisse mittels des Neutrino Weighting Algorithmuses zu rekonstruieren. Hierfür wird die Neutrino Pseudorapiditätsverteilung in Monte Carlo Simulationen für 13 verschiedene Topmassen untersucht. Die Studien wurden sowohl vor, als auch nach Anwendung der Selektionskriterien durchgeführt.

Es wird gezeigt, dass die Pseudorapiditätsverteilung hinreichend genau durch eine Gauß-Verteilung beschrieben werden kann. Die Standardabweichung dieser Verteilung wird als Funktion der Topmasse parametrisiert. Des Weiteren wird eine systematische Abweichung diskutiert, welche darauf hindeutet, dass die Pseudorapiditätsverteilung tatsächlich zwei Peaks enthält. Zudem wird der Einfluss der einzelnen Selektionskriterien auf die Standardabweichung untersucht.

Abschließend wird die Auflösung der fehlenden Energie bestimmt und ebenfalls als Funktion der Topmasse parametrisiert.

Contents

1. Introduction	1
2. The Standard Model of Particle Physics	3
2.1. The Strong Interaction	4
2.2. The Electroweak Interaction	5
2.3. The Higgs Mechanism	5
3. The Top Quark	7
3.1. Production of Top Quark Pairs	7
3.2. Decay of Top Quark Pairs	8
3.3. Properties	11
4. Experimental Setup	13
4.1. The Large Hadron Collider	13
4.2. The ATLAS Coordinate System	14
4.3. The ATLAS Detector	15
5. Reconstruction of Top Quark Pairs in the Dileptonic Channel	19
5.1. The Dileptonic $t\bar{t}$ Decay	19
5.2. Neutrino Weighting	20
6. The Monte Carlo Samples	23
7. Generator Studies	25
7.1. Parton Level Studies	25
7.1.1. Top Quark Mass and Pseudorapidity Distributions	25
7.1.2. Comparison of Neutrino and Antineutrino Distributions	26
7.1.3. Gaussian Fit to the Neutrino Pseudorapidity Distribution	27
7.1.4. The Parameter Dependence on the Top Mass	30
7.2. Event Reconstruction, Selection and Yield	31

Contents

7.3. Reconstruction Level Studies	32
7.3.1. Control Plots for Kinematic Variables	33
7.3.2. Gaussian fit to the Neutrino Pseudorapidity Distribution	36
7.3.3. The Parameter Dependence on the Top Mass	37
7.3.4. Cutflow Analysis	38
7.3.5. The Missing Energy Resolution	40
8. Conclusions and Outlook	43
A. Full List of Cuts in Event Selection	45
B. Literature	47

1. Introduction

Elementary Particle Physics focusses on the search and description of the smallest constituents matter is made of. The foundation of Particle Physics is the Standard Model (SM) which bases on theoretical considerations and describes successfully many experimental observations. Particle accelerators are used to test the predictions of the Standard Model and to open windows for new physics beyond the Standard Model. The newest and most powerful particle accelerator available for scientists all around the world is the Large Hadron Collider (LHC) in Geneva which is the largest machine ever built by humankind.

The LHC allows scientists to study the properties of the top quark - the heaviest known elementary particle discovered at the Tevatron in 1995. Its mass is almost equal to the mass of one atom of tungsten and is a free parameter in the SM. A precise measurement of the mass is needed to test the consistency of the SM, or discover physics beyond the SM. In the proton-proton collisions at the LHC most top quarks are produced in pairs together with an anti-top quark. Each top quark can decay either into a final state of only jets or into a jet together with a lepton and its corresponding (anti-)neutrino.

The treatment of processes which include neutrinos in their final state always poses a challenge, but it can be solved in case of only one neutrino by using total momentum conservation. Thus most top quark research is focused on events where only one top quark decay results in leptons in the final state. Events in which both top quarks decay into leptons - the dileptonic channel - two neutrinos are present in the final state, and the kinematic quantities cannot be calculated by using momentum conservation alone. In this case a method called *neutrino weighting* is used which requires knowledge on the behaviour of neutrinos from top quark decays.

The main part of this thesis describes studies on pseudorapidity distributions of neutrinos to determine a parameterization which is used as an input for the neutrino weighting algorithm in the context of a top mass measurement.

Chapter 2 will give a short introduction into the Standard Model followed by an

1. Introduction

overview on the top quark given in chapter 3. Chapter 4 describes the experimental setup - the LHC and the ATLAS detector. The reconstruction of top quark pairs in the dileptonic channel is discussed in chapter 5. The Monte Carlo samples used in the studies are described in chapter 6. Chapter 7 describes the studies which are performed on generator level and a conclusion is given in chapter 8.

Natural units $\hbar = c = 1$ are used throughout this thesis and all given values for particle properties are taken from [1] unless not otherwise stated.

2. The Standard Model of Particle Physics

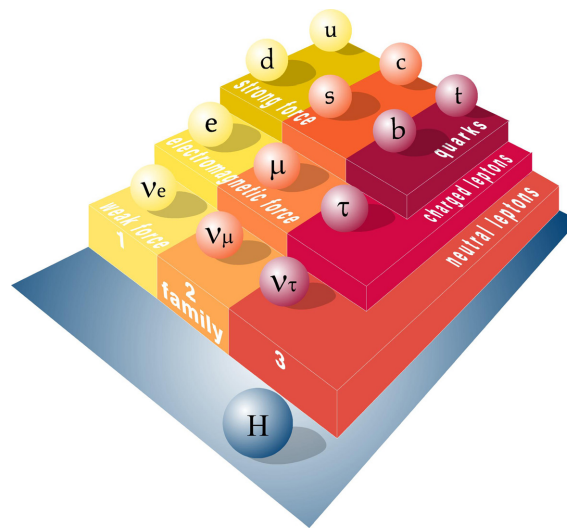


Figure 2.1.: Overview of all known elementary particles [2].

Elementary particles are the basic building blocks of matter, which have no known substructure and are shown in figure 2.1. One distinguishes between quarks and leptons which are all spin-1/2 fermions. All elementary particles discovered so far can be classified into three generations consisting of two quarks and two leptons each. The quantum numbers electric charge (Q) in units of the charge e of the positron, the third component of the weak isospin (I_3) and the weak hypercharge ($Y_W = 2(Q - I_3)$) are assigned to the leptons. One distinguishes charged leptons ($Q = -1$) and neutral neutrinos ($Q = 0$). Quarks are classified by the quantum numbers electric charge (Q), the third component of the weak isospin (I_3) and the hypercharge ($Y = 2(Q - I_3)$). Quarks also carry a color charge (C) and exist as up-type ($Q = +2/3$) and down-type ($Q = -1/3$) quarks. One generation of elementary particles consists of one up-type and one down-type quark together with one

2. The Standard Model of Particle Physics

neutrino and one charged lepton. The first generation contains the up (u) and down (d) quarks, the electron-neutrino (ν_e) and the electron (e). Charm (c) and strange (s) quark alongside the muon-neutrino (ν_μ) and muon (μ) are the particles of the second generation. The third generation is constituted of the top (t) and bottom (b) quark, the tau-neutrino (ν_τ) and the tau (τ). There is an antiparticle for every elementary particle which has the inverted quantum numbers but the same mass. The Standard Model of Particle Physics combines quantum electro- and chromodynamics together with the weak interaction to describe the interactions between the elementary particles. The SM itself does not predict the amount or properties of the particles and can be expressed as a gauge symmetry group:

$$SU(3)_C \times SU(2)_L \times U(1)_Y .$$

2.1. The Strong Interaction

The strong interaction is described by quantum chromodynamics, is given by the gauge symmetry group $SU(3)_C$ and describes the interactions of particles carrying a color charge. The eight generators of $SU(3)_C$ result in eight different gluons. Those are the mediating particles in the strong interaction. Furthermore, they are present in an octet and can couple, unlike the mediating particles of the electromagnetic interaction, to one another because they carry color charges themselves. The so-called *confinement* requires quarks to be bound in colorless hadrons because states with a color charge are not invariant under $SU(3)_C$ transformations. Therefore, quarks cannot be observed as free particles in nature. These colorless hadrons are either mesons $|q\bar{q}\rangle$ combining two quarks carrying a color and the corresponding anticolor charge or baryons $|qqq\rangle$ combining all three colors or anticolors. The strong coupling increases with increasing distance between two quarks which are bound by gluons in contrast to the weak coupling that decreases with increasing distance. If one tries to separate two quarks, there is a point when it is energetically more favorable to produce an additional quark-antiquark pair instead of increasing the distance any further. This is called *hadronization* and is responsible for quarks being measured as jets in detectors.

2.2. The Electroweak Interaction

The electroweak interaction is the unification of quantum electrodynamics and the weak interaction proposed by Weinberg, Salam and Glashow [3–5] and is described by $SU(2)_L \times U(1)_Y$, the combination of the gauge symmetry groups for isospin and hypercharge. The mediating bosons are γ and Z^0 for neutral current processes and W^\pm for charged current processes. While the photon can only couple to particles with $Q \neq 0$, the W^\pm and Z^0 bosons can transform all elementary particles. Due to the V-A structure of the $SU(2)_L$ symmetry group one can find left-handed isospin doublets and right-handed isospin singlets:

$$\begin{pmatrix} \nu \\ l^- \end{pmatrix}_L \quad \begin{pmatrix} u \\ d \end{pmatrix}_L \quad u_R \quad d_R \quad l_R^-.$$

Neutrinos are assumed massless¹ in the SM, thus there are no right-handed neutrino isospin singlets. The charged current interaction given by the $SU(2)_L$ gauge symmetry group allows mixing between different generations of quarks because the weak eigenstates are not equal to the flavour eigenstates [6, 7]. This is described by the unitary CKM matrix which connects the weak down-type eigenstates $|d'\rangle$ to the flavour eigenstates $|d\rangle$:

$$\begin{pmatrix} |d'\rangle \\ |s'\rangle \\ |b'\rangle \end{pmatrix} = \begin{pmatrix} V_{ud} & V_{us} & V_{ub} \\ V_{cd} & V_{cs} & V_{cb} \\ V_{td} & V_{ts} & V_{tb} \end{pmatrix} \cdot \begin{pmatrix} |d\rangle \\ |s\rangle \\ |b\rangle \end{pmatrix}. \quad (2.1)$$

The square of the absolute value for each entry of the CKM matrix gives the probability to find the corresponding quarks in the same W^\pm vertex.

2.3. The Higgs Mechanism

The elementary particles and gauge bosons are defined as massless fields. The SM forbids massive fields which would lead to mass terms in the Lagrangian that would not be invariant under the gauge symmetry transformations. But the non-zero masses of the elementary particles as well as the W^\pm and Z^0 bosons have been measured in experiments. A solution to include massive particles in the SM is given

¹But there is evidence for neutrino oscillation which implies that neutrinos have a small mass [8–10].

2. *The Standard Model of Particle Physics*

by the Higgs mechanism [11, 12] which adds the possibility of spontaneous symmetry breaking and allows masses for the fermions and heavy gauge bosons.

The addition of the Higgs mechanism to the SM yields four additional degrees of freedom. Three of these are used to give masses to the W^\pm and Z^0 bosons. The last degree of freedom introduces a new boson: the Higgs boson. The search for this new boson is one of the main goals of the Large Hadron Collider. On the fourth of July 2012 the ATLAS and CMS collaborations reported that they have found an excess in data of about 5σ each around a mass of 125 GeV [13, 14]. Further analysis of the gathered data improved the statistics and allowed the conclusion that the discovered particle is the Higgs boson [15, 16].

3. The Top Quark

The top quark was discovered in 1995 by the CDF and D0 experiments at the Tevatron [17,18]. In this section, the production of $t\bar{t}$ pairs and their possible decay channels are described. Furthermore, an overview on the properties of the top quark is given.

3.1. Production of Top Quark Pairs

This thesis summarizes studies assuming one of the possible decay channels of a $t\bar{t}$ pair. Therefore, only the pair production will be discussed in this section. The electroweak single top production is described in [19, p. 598].

The main production mechanism of $t\bar{t}$ pairs in hadron colliders is the strong interactions between the gluon and quark components of the colliding particles. The leading order Feynman diagrams are shown in figure 3.1. In contrast to an e^+e^-

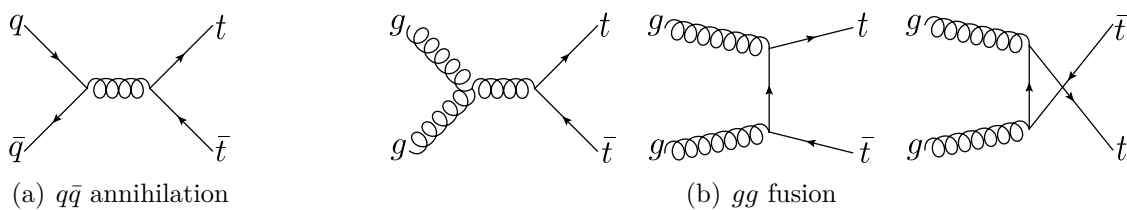


Figure 3.1.: Leading order Feynman diagrams for the $t\bar{t}$ production at hadron colliders via $q\bar{q}$ annihilation (a) and gg fusion (b).

collider, the actual collisions in a pp collider do not happen directly between the accelerated particles. Instead two partons, each from one proton, collide carrying an unknown fraction of the proton momentum. To produce a $t\bar{t}$ pair the effective center-of-mass energy $\sqrt{\hat{s}}$ must exceed $\sqrt{\hat{s}} \geq 2m_t$. By introducing the momentum

3. The Top Quark

fractions of each parton x_i , the effective center-of-mass energy can be written as:

$$\hat{s} = x_1 x_2 s. \quad (3.1)$$

By setting $x_1 \approx x_2$ and using a value for the top mass of $m_t = 173$ GeV, one can calculate typical values for the momentum fraction:

$$\begin{aligned} x &\geq \frac{2m_t}{\sqrt{s}}, \\ &\geq 0.18 && (\text{Tevatron } \sqrt{s} = 1.96 \text{ TeV}), \\ &\geq 0.05 && (\text{LHC } \sqrt{s} = 7 \text{ TeV}). \end{aligned}$$

The probability to find a parton with a certain momentum fraction in the proton is given by the parton distribution function (PDF) $f(x, \mu^2)$ with μ being the energy scale at which they were evaluated [20, p. 10]. Figure 3.2(a) shows the CT10 parton distribution function [21] for $\mu^2 = (2m_t)^2$ and shows that the gluons become the dominating partons for decreasing momentum fractions x . The Tevatron produced approximately 85% of the $t\bar{t}$ pairs via $q\bar{q}$ annihilations and only 15% via gg fusion. As one can see in figure 3.2(a), the LHC produces its $t\bar{t}$ pairs mainly via gg fusion due to the smaller required momentum fraction.

The usage of PDFs does not yield any information for a single event thus the momentum along the beam axis is unknown for a single event.

The $\sigma(pp \rightarrow t\bar{t})$ cross-section measured by the ATLAS collaboration is shown together with the theoretical expectation in figure 3.2(b). The combined result does not include the newest measurements given at the bottom of this figure.

3.2. Decay of Top Quark Pairs

The decay width for the top quark, taking into account next-to-leading order effects, is given by [19, p. 2]:

$$\Gamma_t = \frac{G_F m_t^3}{8\pi\sqrt{2}} \left(1 - \frac{m_W^2}{m_t^2}\right) \left(1 + 2\frac{m_w^2}{m_t^2}\right) \left[1 - \frac{2\alpha_s}{3\pi} \left(\frac{2\pi^2}{3} - \frac{5}{2}\right)\right], \quad (3.2)$$

with the Fermi coupling $G_F = \sqrt{2}g^2/(8m_W^2)$. Evaluated for α_s at the Z^0 scale, this yields a decay width of $\Gamma_t \approx 1.3$ GeV which corresponds to a lifetime of $\tau_t \approx 0.5 \cdot 10^{-24}$ s [19]. This is smaller than the time scale needed for hadronization and

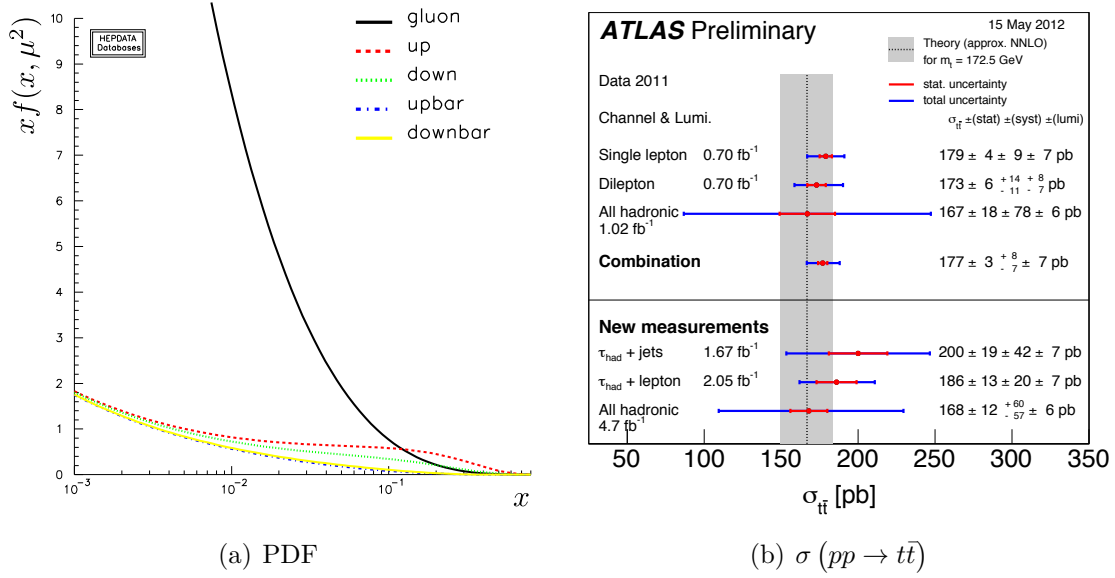


Figure 3.2.: Parton distribution function for $\mu = 2 \cdot 173$ GeV based on [22] (a) and $t\bar{t}$ cross-section measured by the ATLAS collaboration [23] (b).

thus the top quark will decay before it is able to form bound states with other quarks. Therefore, the top quark will decay as a “bare” quark via the weak interaction into a W^+ boson and a down-type quark $t \rightarrow Wq_d$. In principle, this down-type quark can be a down, strange or bottom quark but $|V_{td}|^2$ and $|V_{ts}|^2$ are negligibly small compared to $|V_{tb}|^2 \approx 1$, so the top quark decays almost exclusively into a bottom quark [19, p. 2].

The W^+ boson will either decay into a lepton and the corresponding neutrino or into two quarks. Due to the high energies available in particle accelerators, these quarks are measured as jets in the detector.

The decays of a $t\bar{t}$ pair can be classified by the different combinations of the possible W boson decays as shown in figure 3.3: if both W bosons decay into quarks, the process is called “all jets”, if one W -boson decays into leptons and one into quarks, it is called “leptons+jets”, and it is called “dilepton” channel when both W bosons decay into leptons. The branching ratios for the different channels are visualized in figure 3.4. In case of a hadronic W^+ decay one finds $u\bar{d}$ or $c\bar{s}$ which can be present in three different colors. This yields a total of six different possibilities, so one finds 36 different combinations for an all jets decay of a $t\bar{t}$ pair. The lepton+jets decays combine the six possibilities from hadronic W^\pm decays with three different leptons and the possibility to swap leptonic and hadronic decay which also yield a total of 36

3. The Top Quark

combinations. The dileptonic $t\bar{t}$ decay can exist in nine different combinations and leads to a total of 81 combinations as seen in figure 3.4. Due to the short lifetime of the τ lepton, which will already decay in the inner detector, the term “dilepton” will refer only to decays into electrons or muons from now on.

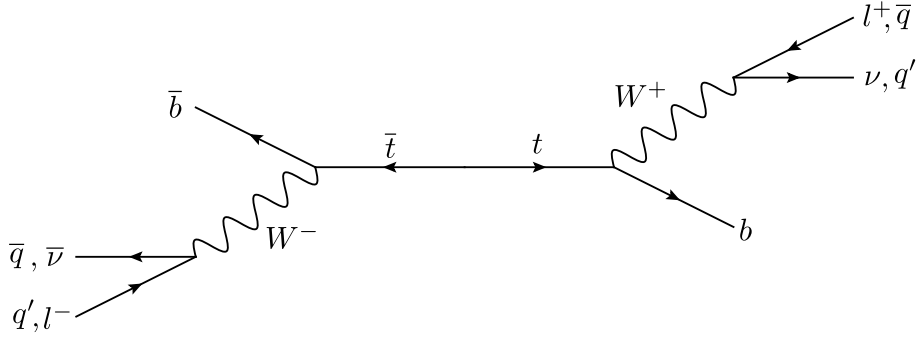


Figure 3.3.: Feynman diagram for the decay of a $t\bar{t}$ pair with all possible W boson final states.

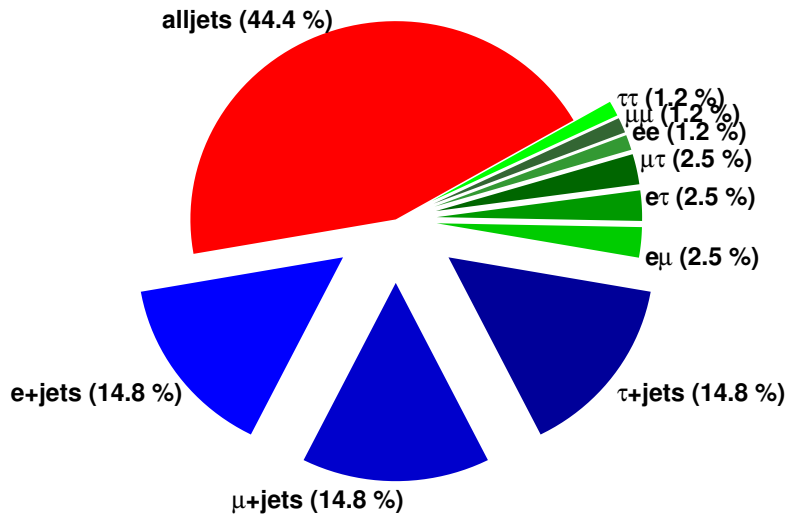


Figure 3.4.: Different decay channels for a $t\bar{t}$ pair with their theoretical branching ratios calculated from combinatorics of quark and lepton assignments under the assumption that universality of the weak interaction holds.

3.3. Properties

This section will discuss the unique properties and present the most precise measurements for the mass of the top quark. As already stated in the previous section, the top quark is the only quark which decays before it is hadronized into mesons or baryons by the strong interaction.

Like all other up-type quarks, the top quark carries a electric charge of $Q = +2/3$. Due to unknown assignment of the products in $t\bar{t}$ decays the possibility for a $Q = +4/3$ was studied but excluded by the four experiments D0, CDF, CMS and ATLAS. The ATLAS results are given in [24].

Another outstanding property of the top quark is its mass which is significantly heavier than the mass of all other known elementary particles and lies in the region of heavy atoms like tungsten. Furthermore, the top mass is larger than the mass of the W boson. This is not the case for all other fermions and thus the top quark is the only elementary particle which is able to decay via a real W boson.

The most precise value for the top mass with a uncertainty of only 0.5% was measured at the Tevatron [25]:

$$m_t = 173.2 \pm 0.9 \text{ GeV.} \quad (3.3)$$

This result is the combination of measurements in the three different channels. The most precise single measurement was made in the lepton+jets channel by the CDF experiment [25, p. 10]. The uncertainties obtained in measurements in the dilepton channel are almost three times as large as in the leptons+jets channel.

This is explained by the two neutrinos in the final state of the dilepton channel which poses a challenge in the event reconstruction. These challenges will be explained in chapter 5 together with a possible solution and the preliminary studies that are needed to extract the top mass in the dilepton channel at the ATLAS experiments. These preliminary studies are the topic of this thesis.

Besides the mass and charge of the top quark, there are many other properties that can be studied in $t\bar{t}$ decays like the helicity of the W boson [26], the spin correlation [27] and the charge asymmetry [28].

4. Experimental Setup

4.1. The Large Hadron Collider

The LHC [29] is located at the CERN research center in Geneva and is the world's most powerful particle accelerator in terms of center-of-mass energy. Its main operation mode is the collision of protons but it is also able to collide lead ions. The protons are injected into the main accelerator ring with a circumference of 27 km after passing several preaccelerators. The LHC was designed for a center-of-mass energy of $\sqrt{s} = 14$ TeV but operated at $\sqrt{s} = 7$ TeV between 2010 and 2012. The LHC has been running at $\sqrt{s} = 8$ TeV since April 2012.

The protons are grouped into bunches with a bunch crossing rate of 40 MHz. A key quantity for any particle accelerator is the rate of events expressed by the instantaneous luminosity \mathcal{L} . This quantity relates the measured event rate \dot{N} of a certain process to the corresponding cross-section σ , the experimental acceptance A and the efficiency ε of the measurement:

$$\mathcal{L} = \frac{\dot{N}}{\sigma A \varepsilon} \quad \left[\frac{1}{\text{cm}^2 \text{s}} \right]. \quad (4.1)$$

This instantaneous luminosity does not depend on the process that was used to measure it. The total number of expected events from a process with the cross-section σ can now be calculated as $N = \sigma A \varepsilon \int \mathcal{L} dt$. Figure 4.1 shows the instantaneous and integrated luminosity recorded with the ATLAS experiment.

Besides the multi-purpose ATLAS detector, the LHC hosts five additional experiments: the CMS experiment which uses another multi-purpose detector, the LHCb experiment which focuses on b physics. Particles with a large pseudorapidity are studied by the LHCf and TOTEM experiments and the research on heavy ions is performed with the ALICE experiment.

The next sections will describe the coordinate system and the detector that is used by the ATLAS experiment.

4. Experimental Setup

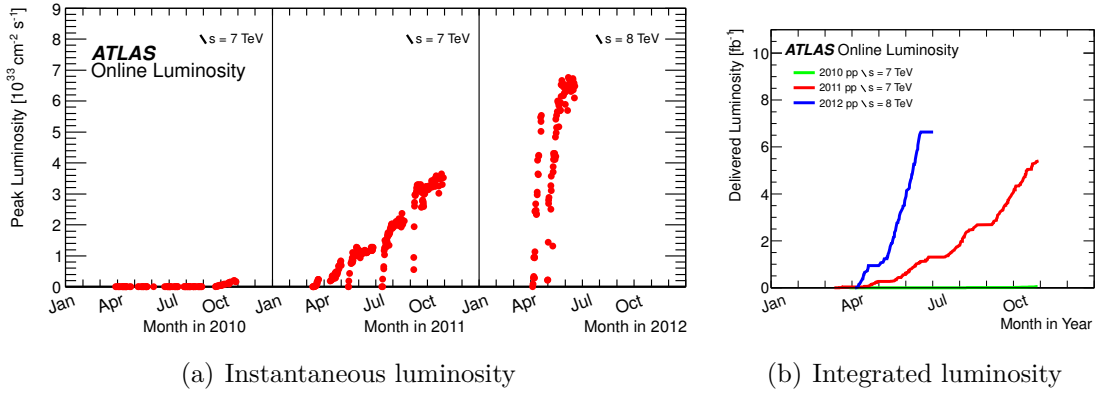


Figure 4.1.: Luminosity for the ATLAS detector until 2.7.2012 [30].

4.2. The ATLAS Coordinate System

The ATLAS collaboration uses a right-handed coordinate system with the z -axis pointing along the beam axis, the x -axis being directed towards the center of the main accelerator ring, the y -axis points upwards. Each particle is described by a four-momentum vector that contains the energy E and the spatial momentum $\vec{p} = (p_x, p_y, p_z)$ of the particle:

$$p = (E, p_x, p_y, p_z). \quad (4.2)$$

The angle φ is measured to the positive x -axis in the plane perpendicular to the beam axis, the angle θ to the positive z -axis and the transverse momentum p_T is defined as:

$$p_T = \sqrt{p_x^2 + p_y^2}. \quad (4.3)$$

Instead of the angle θ , the pseudorapidity η is often used to describe the angle of a particle to the beam axis:

$$\eta := -\ln \left[\tan \left(\frac{\theta}{2} \right) \right] = \frac{1}{2} \ln \left[\frac{|\vec{p}| + p_z}{|\vec{p}| - p_z} \right]. \quad (4.4)$$

For particles whose masses are negligible compared to their energies, $|\vec{p}| \approx E$ holds and the pseudorapidity η is equal to the rapidity y :

$$y = \frac{1}{2} \ln \left[\frac{E + p_z}{E - p_z} \right]. \quad (4.5)$$

The rapidity y is a parameter of the special relativity that parameterizes the boost into a system where the object does not move in z -direction. Thus the pseudorapidity and rapidity cannot be invariant under Lorentz transformations but differences are invariant. The Cartesian coordinates can now be expressed via the following equations:

$$p_x = p_T \cos \varphi, \quad (4.6)$$

$$p_y = p_T \sin \varphi, \quad (4.7)$$

$$p_z = p_T \sinh \eta. \quad (4.8)$$

4.3. The ATLAS Detector

The ATLAS (**A** toroidal **LHC** apparatus) detector [31] has a cylindric shape around the LHC beam axis. It is 25 m in height and width, and 44 m in length with a total weight of 7000 tonnes. The detector consists of different layers of subdetectors which are used to measure different types of particles. These layers are cylindric themselves as can be seen in figure 4.2.

The inner detector consists of a silicon pixel detector, a semiconductor tracker (SCT) and a transition radiation tracker (TRT). It covers a range of $|\eta| < 2.5$ and is surrounded by a solenoid magnet that produces a magnetic field of 2 T inside the inner detector. The pixel detector is in close proximity to the beam axis and is used to determine the position of the vertices from the particle hits in the different pixel layers. The track of a charged particle is bent by the magnetic field. Therefore, the momentum can be calculated from measurements of the track curvature in the SCT and TRT.

The electromagnetic calorimeter covers a region of $|\eta| < 3.2$ and consists of electrodes combined with lead absorbers and interleaved by liquid argon. An electromagnetically interacting particle deposits its energy in the lead absorbers and produce a shower that ionises the liquid argon. Due to the electric field created by the electrodes, the ionised argon atoms and electrons will drift towards these electrodes

4. Experimental Setup

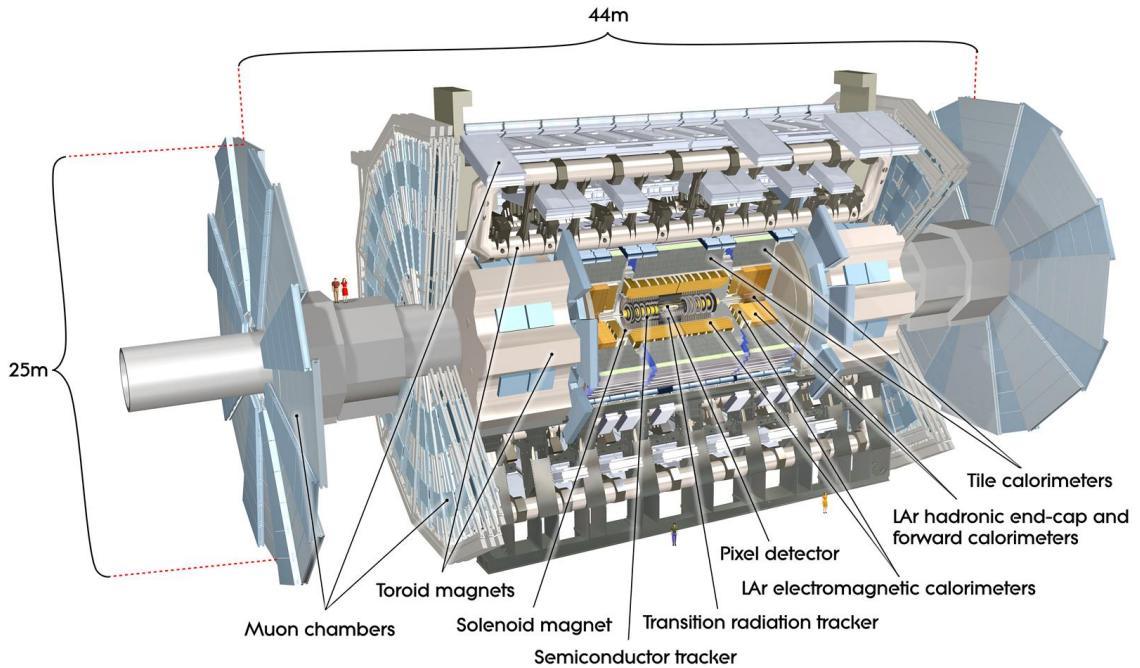


Figure 4.2.: Schematic overview of the ATLAS detector showing the different layers [32].

and induce a charge while drifting as described by Ramo's theorem [33]. The total induced charge is equal to the charge produced in the ionisation and it is thus dependent on the energy of the particle.

The hadronic calorimeter is used to measure the energy of hadrons that were able to traverse the electromagnetic calorimeter. In the barrel region, $|\eta| < 1.7$, it consists of iron plates interleaved by plastic scintillator tiles. An incoming particle will shower in the iron plates, the produced charged particles will excite the scintillator which emits photons. These light pulses are carried to photomultiplier tubes by optical fibres. To improve radiation hardness a copper absorber with liquid argon as sampling medium is used in the end-cap region $1.5 < |\eta| < 3.2$. Close to the beam axis ($3.1 < |\eta| < 4.9$) the absorber is replaced by high density copper and tungsten. Muons with energies in the GeV region only deposit a small amount of their energy in the calorimeters because they are MIPs (minimum ionising particles). To measure the track and momentum of muons, drift chambers surround the hadronic calorimeter. These muon chambers are immersed in a 4 T magnetic field which is produced by toroidal magnets and are used to measure the momentum of the muons.

There are approximately 20 events per bunch crossing¹ in the detector and thus the event rate lies in the region of 1 GHz. This yields a total raw data rate in the region of Petabytes/sec which is several orders of magnitude larger than the rates which are technically possible to store permanently. Furthermore, the majority of processes, for example elastic scattering between protons, is not useful for the analysis. To reduce the data rate, a three level trigger system is used to select and store only interesting processes. The Level-1 trigger reduces the event rate to approximately 75 kHz by checking for hits in the electromagnetic calorimeter and the muon chamber. After the Level-1 trigger is passed the event is buffered and processed by the following two triggers which reduce the event rate to about 200 Hz. This rate can be stored on hard disks and be analysed offline.

¹Also referred to as pile-up in the detector.

5. Reconstruction of Top Quark Pairs in the Dileptonic Channel

As mentioned before, the branching ratio for the dileptonic $t\bar{t}$ decay is relatively small compared to the ones for the all jets or lepton+jets channels and the majority of top quark research is done in the lepton+jets channel. Nevertheless, the dilepton channel allows the study of interesting effects like the spin correlation of $t\bar{t}$ pairs and is also used in studies to check for consistency with the other channels. Furthermore, this channel has a good signal to background ratio due to the unique signature of the final state particles.

5.1. The Dileptonic $t\bar{t}$ Decay

The final state consists of two b quarks, two charged leptons and the two corresponding neutrinos. Even though the initial momenta in z -direction for the two partons in a pp collision are unknown, there is no momentum component in the plane perpendicular to the beam axis. Due to momentum conservation in each direction, there cannot be any momentum component in this plane after the reaction. Therefore, the sum of all particle momenta in the x - and y -direction has to be zero. If this is not the case one defines the missing amount of momentum as the missing transverse momentum, MET .

The signature of a dileptonic $t\bar{t}$ decay comprises two jets (both of which stem from a b quark), two high p_T isolated leptons and large missing transverse momentum due to the two neutrinos.

A total of six particles in the final state, each described by a four-momentum vector, results in 24 degrees of freedom (dof) that have to be determined to fully reconstruct the $t\bar{t}$ pair. One can measure the components of the four-momentum vectors for the charged leptons and the (b -)jets which leaves eight degrees of freedom. Additionally, two constraints come from the MET measurements in both directions which are the

5. Reconstruction of Top Quark Pairs in the Dileptonic Channel

result of the neutrino momenta in the corresponding direction:

$$p_{\nu,x/y} + p_{\bar{\nu},x/y} = MET_{x/y}. \quad (5.1)$$

Another two equations (5.2) are obtained from the fact that the W^\pm bosons are real instead of virtual particles:

$$\left(p_{\nu_{1/2}} + p_{l_{1/2}}\right)^2 = m_W^2 \quad (5.2)$$

The last conditions are obtained by the assumptions that the masses for the top and anti-top quark are equal and the approximation of massless neutrinos which is valid at the energy and length scales of high energy physics experiments.

After combining all constraints and measurements, one dof is still left that cannot be determined by the event kinematics. A method called *neutrino weighting* allows to reconstruct the top quark mass by identifying the best combination of mass hypotheses and neutrino four-momenta as explained in the next section.

The main background process which mimics the same signature is the Drell-Yan process $Z/\gamma + \text{jets}$ where the photon or Z boson decays into leptons. Other possible background processes are the $W + \text{Jets}$, the $t\bar{t}$ lepton+jets or single top decays with an additional lepton. These fake leptons are either particles that are misidentified as leptons or non-prompt leptons which originate from another process.

5.2. Neutrino Weighting

The neutrino weighting algorithm allows to obtain a solution for the underconstrained events given by dileptonic $t\bar{t}$ decays: In order to eliminate the last degree of freedom, one assumes a top mass m_t and values of the pseudorapidities for both neutrinos. The measured MET for the x - and y -direction is not used directly by the reconstruction, but as a cost function as describes in the following.

The kinematics of the system can now be solved and the four-momenta of the neutrinos calculated [34, pp. 85-87]. Due to multiple quadratic equations there are up to eight different solutions. The solutions for neutrino and antineutrino are used to calculate the expected per event missing transverse momentum:

$$E_{x/y}^{calc} = (p_\nu + p_{\bar{\nu}})_{x/y}. \quad (5.3)$$

In an ideal world it would be possible to find the perfect combination of top mass assumptions and chosen neutrino pseudorapidities so that $E^{calc} = MET$. However, this is not possible due to experimental uncertainties of the MET . Instead, one assumes that the calculated E^{calc} for each direction has a Gaussian uncertainty $\sigma_{\cancel{E}}$, the so-called missing transverse energy resolution. A cost function, or weight, is then calculated based on the deviation between the predicted and measured MET :

$$\omega(m_t) = \sum_{\eta_1 \times \eta_2} \sum_{sol.} \exp\left(-\frac{(E_x^{calc} - MET_x)^2}{2\sigma_{\cancel{E}_x}^2}\right) \exp\left(-\frac{(E_y^{calc} - MET_y)^2}{2\sigma_{\cancel{E}_y}^2}\right). \quad (5.4)$$

This weight is calculated for every top mass assumption by taking the first sum over a grid of chosen neutrino pseudorapidity combinations for both neutrinos and the second one over all possible solutions for the specific $\eta_\nu, \eta_{\bar{\nu}}$ and m_t combination.

To successfully calculate a value for the weight one has to determine the missing energy resolution and a grid of pseudorapidity assumptions which is described in this thesis. The pseudorapidity grid should be chosen such that each bin contains approximately the same number of events to avoid different statistics for different bins. Therefore, it is necessary to study the neutrino pseudorapidity distribution whose width slightly depends on the top mass.

A value for the top mass can be extracted from this weight by using a maximum likelihood method [34, p. 56ff].

6. The Monte Carlo Samples

This chapter describes the Monte Carlo (MC) samples that are used in the preliminary studies on the neutrino pseudorapidity distribution and the missing energy resolution.

The simulated $t\bar{t}$ samples were created by MC@NLO [35] and take into account the next-to-leading order effects. The used samples are called *nonallhadronic* and include the leptons+jets and the dilepton channels. Quarks in the final state of a process can emit additional gluons which themselves are able to emit more gluons or to split into a quark pair. In principle, these parton showers are higher order corrections for the leading process but are not calculated exactly. Alternatively, they are simulated by using the cluster fragmentation model implementation of HERWIG [36] with the AUET2-CT10 tune. In the collision of protons, one parton of each proton will interact in the $t\bar{t}$ production process. Nevertheless, the rest of the proton participates in additional processes. These processes form the underlying events that are modeled by JIMMY [37] in the samples that are used.

Samples that can be compared to real data are produced by simulating the detector response with GEANT4 [38]. This response is reconstructed like measured data by using the same ATLAS reconstruction software [39]. The final sample consists of these reconstructed data but provides the truth information of the MC@NLO generator so that e.g. neutrino distributions can be studied.

A total of 13 samples with different top masses are used in this thesis:

$$m_t \text{ [GeV]} \in \{140, 150, 160, 165, 167, 170, 172.5, 175, 177, 180, 190, 200, 210\}.$$

In addition to all particles on reconstruction and parton level, the samples also contain information on their decay type and channel. The event is required to be a true dileptonic $t\bar{t}$ decay throughout the following studies.

7. Generator Studies

This chapter summarizes the analysis of Monte Carlo samples and pseudorapidity distributions of neutrinos. The steps of this analysis are explained for the parton level MC data and, after an event selection, are repeated on the reconstruction level.

7.1. Parton Level Studies

The parton level data is analysed in this section. All plots were created using the MC@NLO weights obtained from the generator. If it is not explicitly mentioned that the plots correspond to neutrino or antineutrino distributions, the shown distributions contain the combined data (see section 7.1.2). Additionally, all distributions have been normalized to one. As stated before, neutrinos cannot be detected and so all information on the neutrino kinematics is taken from the truth information. The first part of the analysis will focus on the top quark pseudorapidity distribution which is needed for the following discussion on the pseudorapidity distribution for neutrinos.

7.1.1. Top Quark Mass and Pseudorapidity Distributions

On parton level, there should not be any differences for the top quark distributions (η , p_T , φ , m) between different channels. The deviations in the generated data are negligible and can be explained with fluctuations. Figure 7.1 shows the mass and pseudorapidity distributions for the lightest (140 GeV) and the heaviest (210 GeV) studied top masses in the ee channel¹.

In the collision of two identical and unpolarized particles with the same energy there is no preferred spatial direction and thus the pseudorapidity distributions of the top and antitop quark should be symmetric around $\eta = 0$. As already stated in section 3.1, the actual reactions which produce $t\bar{t}$ pairs happen between two partons

¹MC status code 123 is used for the top truth information.

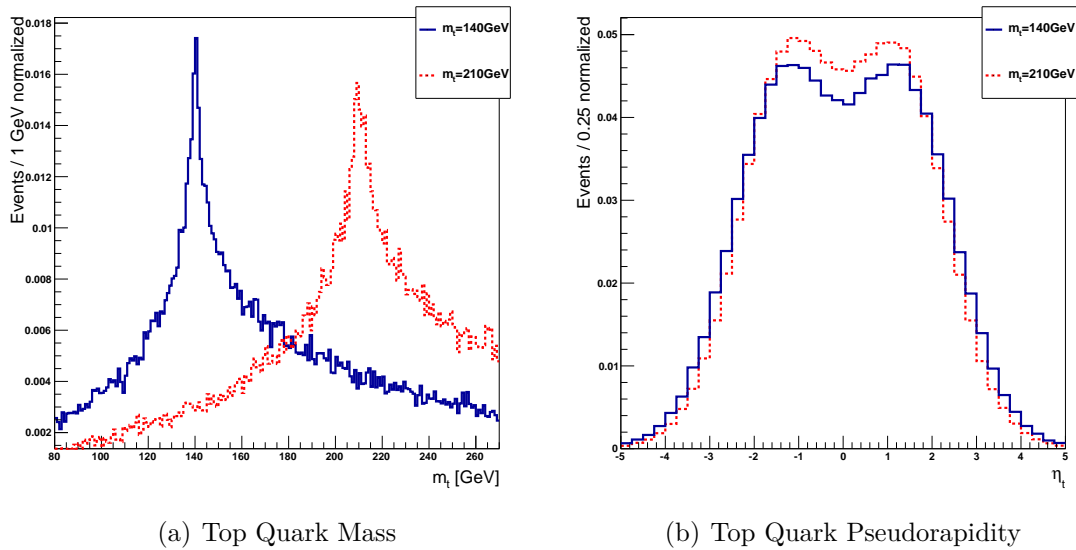


Figure 7.1.: The mass (left) and pseudorapidity (right) distributions for $m_t = 140$ GeV and $m_t = 210$ GeV in the ee channel. The difference in the distributions for the $e\mu$ and $\mu\mu$ channel is negligible.

and not between the protons directly. These partons carry a fraction of the proton momentum described by the PDF. The two peaks in figure 7.1(b) are a result of the fact that an asymmetric collision between a parton with a smaller and one with a higher momentum fraction is more likely than the collision between two partons with the same fraction as can be seen in figure 3.2(a). This asymmetric collision leads to a boosted $t\bar{t}$ system which explains the two peaks. At the Tevatron, $t\bar{t}$ pairs are produced almost at rest. The η -distribution thus peaks at 0. In pp accelerators with higher center-of-mass energies than the LHC uses, both peaks in 7.1(b) are more distinct because an even smaller momentum fraction for one of the gluons is possible at the same momentum transfer. Instead of higher energies the same behaviour can also be observed for smaller top masses. In figure 7.1(b) the peaks for $m_t = 140$ GeV are more distinct, especially the difference between the local minimum at $\eta = 0$ and the value at the peaks is larger than the one for the larger top mass $m_t = 210$ GeV.

7.1.2. Comparison of Neutrino and Antineutrino Distributions

The dileptonic $t\bar{t}$ decay always has a neutrino and an antineutrino in its final state. These can either have the same flavour in case of the ee or $\mu\mu$ channel or have a different flavour in the $e\mu$ channel. In the following section it is checked whether

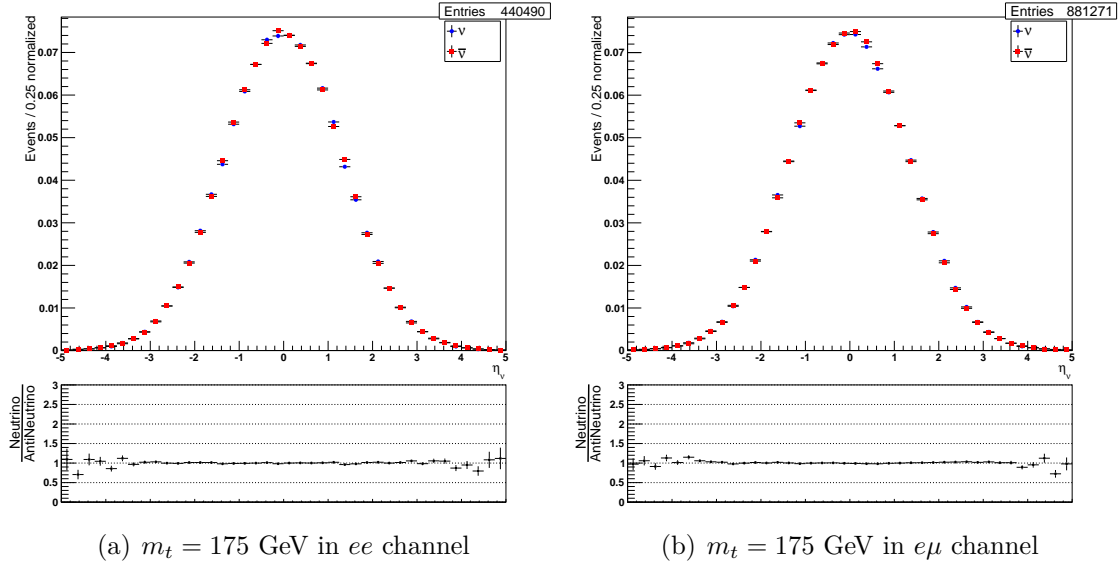


Figure 7.2.: Normalized neutrino and antineutrino distributions(top) and the per bin ratio of the number of neutrinos divided by the number of antineutrinos (bottom)

the pseudorapidity distributions for neutrino and antineutrino have to be described separately if they can be merged. Figure 7.2 shows both distributions for two top mass-channel combinations as an example but the discussion and analysis holds for all 39 combinations. It can be seen in the plots that the deviation between both distributions is negligible in the central region for $|\eta| < 3$ with the ratio being very close to one. The tails in both distributions, $3 < |\eta| < 5$, have deviations up to $\approx 30\%$ due to the fluctuations which are caused by the small number of entries in the corresponding bins. Additionally, there is no systematic or periodic discrepancy of the ratio compared to one for the full η range. This allows the conclusion that it is sufficient to discuss the combined distributions for the neutrino pseudorapidity. Furthermore, one gains increased statistics which improves the obtained parameterization.

7.1.3. Gaussian Fit to the Neutrino Pseudorapidity Distribution

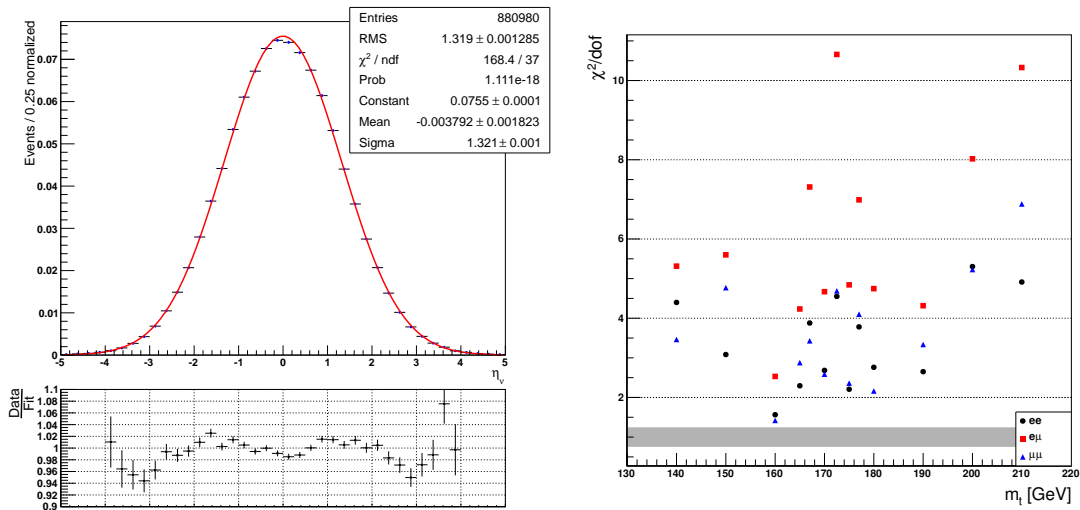
The neutrinos in the dileptonic $t\bar{t}$ decay always originate from one W boson which is the direct decay product of one top quark. Thus the neutrinos should at least loosely follow the direction of the top quark and show a similar pseudorapidity distribution

7. Generator Studies

as the one shown in figure 7.1(b). However, as one could already see in figure 7.2, the distribution has only one clearly visible peak. A Gaussian distribution (7.1) was fitted to the data and is described by the constant C , the standard deviation σ and the mean value $\langle\eta\rangle$. The result for one top mass and channel combination is given in figure 7.3(a) as an example.

$$P(\eta) = C \cdot \exp\left[-\frac{(\eta - \langle\eta\rangle)^2}{2\sigma^2}\right] \quad (7.1)$$

The reduced χ^2 values for all top mass and channel combinations is shown in

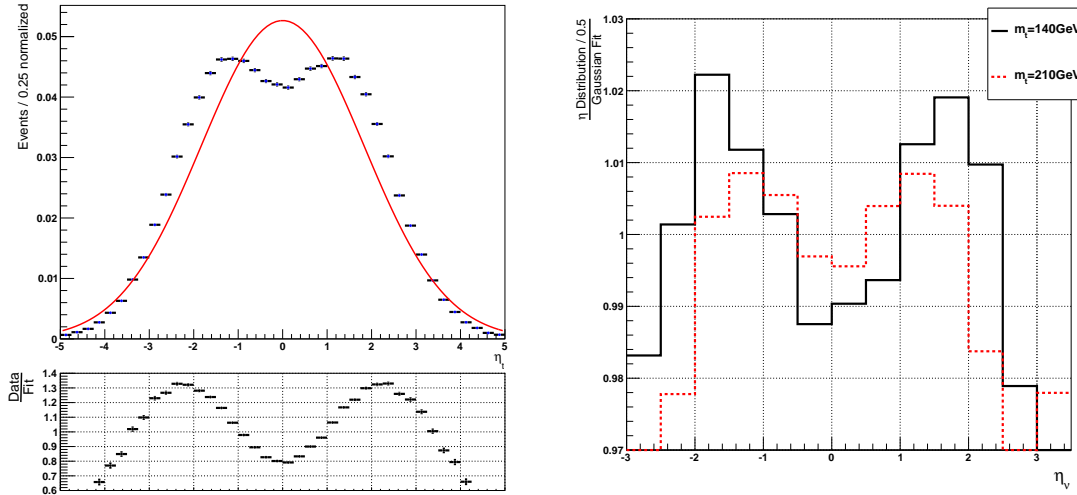


(a) Gaussian fit to the η -distribution for $m_t = 172.5$ GeV in the ee channel. (b) Reduced χ^2 values with one sigma level.

Figure 7.3.: Analysis of the Gaussian fits to the neutrino pseudorapidity distributions on parton level. On distribution is given as an example (a) and the reduced χ^2 of all fits is shown (b).

figure 7.3(b). Not a single value lies within the one sigma region given by the χ^2 -distribution. This is not unexpected since the Gaussian assumption for the pseudorapidity distribution has no physical motivation behind it. Additionally, the relative uncertainty per bin, which is $\propto 1/\sqrt{N}$, is basically zero due to the large number of events on parton level and thus contributes to the large values for the reduced χ^2 . The ratio of the pseudorapidity distribution and the Gaussian fit (figure 7.3(a), bottom) shows a systematic deviation around one. At $\eta \approx 0$ the ratio lies below and for the flanks $1 < |\eta| < 2$ above one. The same behaviour can be found in all channels

and for all top masses. It can be explained by looking at the results of a Gaussian fit into a distribution which contains two peaks. To illustrate this, a fit was performed to the top quark pseudorapidity distribution and is shown in figure 7.4(a). In the central region the ratio lies again below and for flanks, which are here $2 < |\eta| < 3$, above one. Figure 7.4(b) shows the ratio for the lightest $m_t = 140$ GeV and heaviest $m_t = 210$ GeV top mass that was studied. As can be seen in this plot, the effect is



(a) Gaussian fit to the top quark η distribution (b) Ratio of neutrino η distribution and Gaussian fit as in figure 7.3(a) bottom

Figure 7.4.: Deviation between the pseudorapidity distributions and the Gaussian fit.

larger for the lighter top mass. Both peaks that can be seen in 7.4(b) have a greater distance and the difference between the ratio in the central region and the one at the peaks is larger. This is consistent with the results for the dependence of the top quark pseudorapidity distribution. Thus the neutrino pseudorapidity indeed loosely follows the top pseudorapidity and has no perfect Gaussian shape. The neutrino η -distribution is the result of folding the top quark η distribution with the angular distributions for the top and W decay and thus smeared out. However, the deviation is at most 2% so the neutrino pseudorapidity can be sufficiently well described by a Gaussian fit. The next step is the determination of a parameterization for C , σ and $\langle \eta \rangle$ that allows to calculate the η grid for any top mass assumption in the neutrino weighting algorithm and is therefore described in the next chapter.

7.1.4. The Parameter Dependence on the Top Mass

The constant C which describes the value of the distribution for $\eta = \langle \eta \rangle$ could be obtained from the fits as seen in figure 7.3(a). But it is more convenient to determine C by normalizing the Gaussian fit, because this fit will only be used as a probability density to calculate the η grid and the coefficient is thus given by $(\sigma\sqrt{2\pi})^{-1}$.

As discussed previously, all pseudorapidity distributions are expected to be sym-

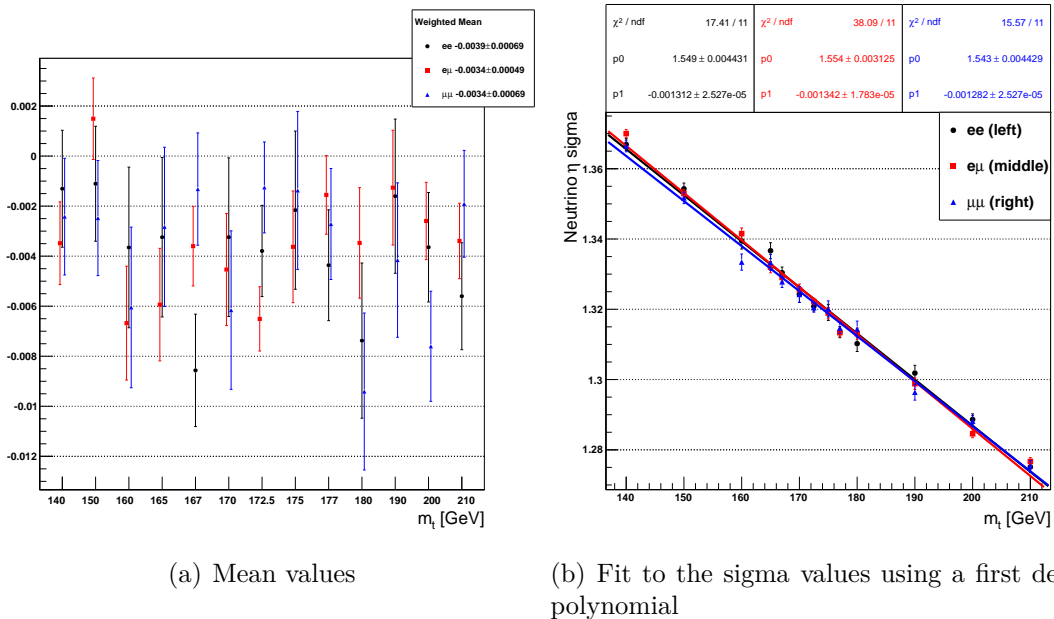


Figure 7.5.: Dependence on top mass of the parameters obtained the Gaussian fit to the neutrino pseudorapidity distribution

metric around $\eta = 0$. The mean values $\langle \eta \rangle$ obtained from the Gaussian fits are shown in figure 7.5(a) for all top mass and channel combinations. There is no dependence on the top mass that can be seen in this plot. Furthermore, all mean values are close to zero but most of them are not consistent with zero. The weighted mean per channel, also given in 7.5(a), is also not consistent with zero. Almost all mean values are negative and do not spread evenly around zero. This effect is also present in the underlying histograms for the neutrino and antineutrino pseudorapidity and should be investigated in future studies. Nevertheless, all obtained fits for the mean are of the order of magnitude $\mathcal{O}(10^{-3})$ and are negligible compare to the width of the distribution $\mathcal{O}(1)$. This allows the conclusion that the value can be fixed to $\langle \eta \rangle = 0$ in the fits to reduce the number of parameters.

The last parameter that is needed to describe the Gaussian is the standard deviation σ . All σ values are plotted over the different top masses in figure 7.5(b). There is no difference in σ between the different channels aside from statistical fluctuations. The value of sigma decreases with an increasing top mass. This means that the pseudorapidity distribution is wider for smaller top masses thus the probability to find higher values of η is slightly increased. The neutrinos are more boosted which is again consistent with the fact that the neutrinos loosely follow the top quarks direction.

In the neutrino weighting algorithm the weight is calculated for different top mass assumptions. Instead of generating a top mass sample for each assumption to determine the σ value directly, one uses a first degree polynomial fit (7.2) to parametrize σ as a function of the top mass m_t :

$$\sigma(m_t) = p_1 \cdot m_t + p_0. \quad (7.2)$$

The obtained values are shown in figure 7.5(b) for each channel separately. The final parameterization $\sigma(m_t)$ after combining the different channels is given by:

$$\sigma(m_t) = (-1.32 \pm 0.02) \cdot 10^{-3} \cdot m_t[\text{GeV}] + (1.550 \pm 0.003). \quad (7.3)$$

7.2. Event Reconstruction, Selection and Yield

To determine a parameterization that can be used on data one has to repeat the analysis on the reconstruction level. The same event selection as used on real data has to be applied to the Monte Carlo samples.

The cuts explained here are also described and used in [40,41]. Electrons are identified by combining the energy measurements in the electromagnetic calorimeter with the track of a charged particle in the inner detector. The electrons, which originate from a real W boson are required to have a transverse momentum of $p_T > 25$ GeV. Due to the range covered by the inner detector, they are additionally required to have a pseudorapidity of less than $|\eta| < 2.47$. The η -region of the transition between barrel and end-cap electromagnetic calorimeters is given by $1.37 < |\eta| < 1.52$ and also excluded.

Muons are reconstructed by fitting tracks measured in the muon chambers. They are required to have $p_T > 20$ GeV and $|\eta| < 2.5$ and a rejection of cosmic muons is applied. After these criteria have been applied to electrons and muons, one demands

7. Generator Studies

exactly two leptons in the final state, either ee , $e\mu$ or $\mu\mu$. Both of these leptons must have opposite charges, be isolated and one of them has to match the trigger lepton. Furthermore, electron and muon tracks must not overlap in the detector. Both leptons have to match with the truth leptons from the $t\bar{t}$ decay.

Jets are reconstructed by using the anti- k_T algorithm [42] and are required to have a transverse momentum of at least $p_T > 25$ GeV and a pseudorapidity of $|\eta| < 2.5$. Additionally, they are excluded if they lie within $\Delta R := \sqrt{\Delta\eta^2 + \Delta\phi^2} < 0.4$ of a successfully reconstructed electron. There have to be at least two such jets in every event, but they are not required to be b -tagged. After the object reconstruction and selection, one sorts the leptons and jets separately by their transverse momenta with the highest p_T object being called the leading jet or lepton.

The missing transverse momentum MET is calculated by using topological clusters and taking into account the presence of the above mentioned reconstructed objects [43].

Alongside the thresholds for the transverse momentum of leptons and jets, one applies cuts to the topological variables MET , H_T and M_{ll} . The dilepton mass $M_{ll} := \sqrt{(p_{l_1} + p_{l_2})^2}$ is defined as the invariant mass of the sum of both lepton four-momenta and H_T is the scalar p_T sum of all reconstructed and selected leptons and jets.

In the ee and $\mu\mu$ channel one requires $MET > 60$ GeV and $|M_{ll} - 91.2 \text{ GeV}| > 10$ GeV to exclude Z +jets background events. Furthermore, a low mass cut of $M_{ll} > 15$ GeV is applied which also reduces the low mass resonance backgrounds (Υ , J/ψ).

These cuts are not used in the $e\mu$ channel, but H_T has to be at least $H_T > 130$ GeV here. The full list of cuts is given in appendix A.

The number of events which passed the object reconstruction and event selection are given in table 7.1. Only 7.4% of the total number of $t\bar{t}$ events were reconstructed and selected. The reconstruction level data is now analysed in the following section.

7.3. Reconstruction Level Studies

This section will discuss the same analysis that was done on parton level. Furthermore, the results of a cutflow analysis are presented and a value for the missing energy resolution is determined. Throughout this section, the neutrino and antineu-

m_t [GeV]	ee channel		$e\mu$ channel		$\mu\mu$ channel	
	P	R	P	R	P	R
140	293863	5537	589685	75952	294306	25797
150	294412	6519	587744	87484	293686	30295
160	146906	3798	293632	48573	146747	17096
165	147158	4047	294413	51387	147509	17874
167	293839	7992	588420	99011	294170	33270
170	147245	4461	294135	53679	146899	18695
172.5	440490	13155	881271	158613	441349	55091
175	147199	4608	292253	55730	146731	19710
177	293435	9497	587692	113046	293993	39741
180	147778	4948	294403	55956	146554	18489
190	147082	5480	266479	62005	146479	22253
200	286108	11553	570868	126347	284831	44702
210	293316	13186	588107	136876	293588	47060

Table 7.1.: Total number of events on parton (P) and reconstruction (R) level for every top mass and channel combination.

trino pseudorapidity distributions have been merged because their difference is again negligible. Furthermore, all shown distributions have been normalized to one again.

7.3.1. Control Plots for Kinematic Variables

Before the actual analysis one checks that the leptons and jets have been reconstructed without any artefacts and the event selection has been applied correctly. Figure 7.6 and 7.7 show these control plots for the $m_t = 172.5$ GeV sample in the ee and $e\mu$ channel as an example, but all discussions and results are again studied for all other top mass and channel combinations. The kinematic plots for the leading electrons and jets transverse momentum and pseudorapidity are given alongside the plots for the topological variables MET , H_T and M_{ll} . All cuts discussed in the event selection were applied. The leading electron η distribution (figure 7.6(a)) does not show zero events in the transition region of barrel and end-cap calorimeters due to the binning of the histogram. The same reason produces the steps in the Z^0 window cut in the dilepton mass distribution (figure 7.6(e)). The transverse momentum cut cannot be seen for the leading electron and jet p_T in figure 7.6(b) and 7.6(c), however the sharp drop to zero below $p_T = 25$ GeV is present in the p_T distributions for the second leading electrons and jets.

7. Generator Studies

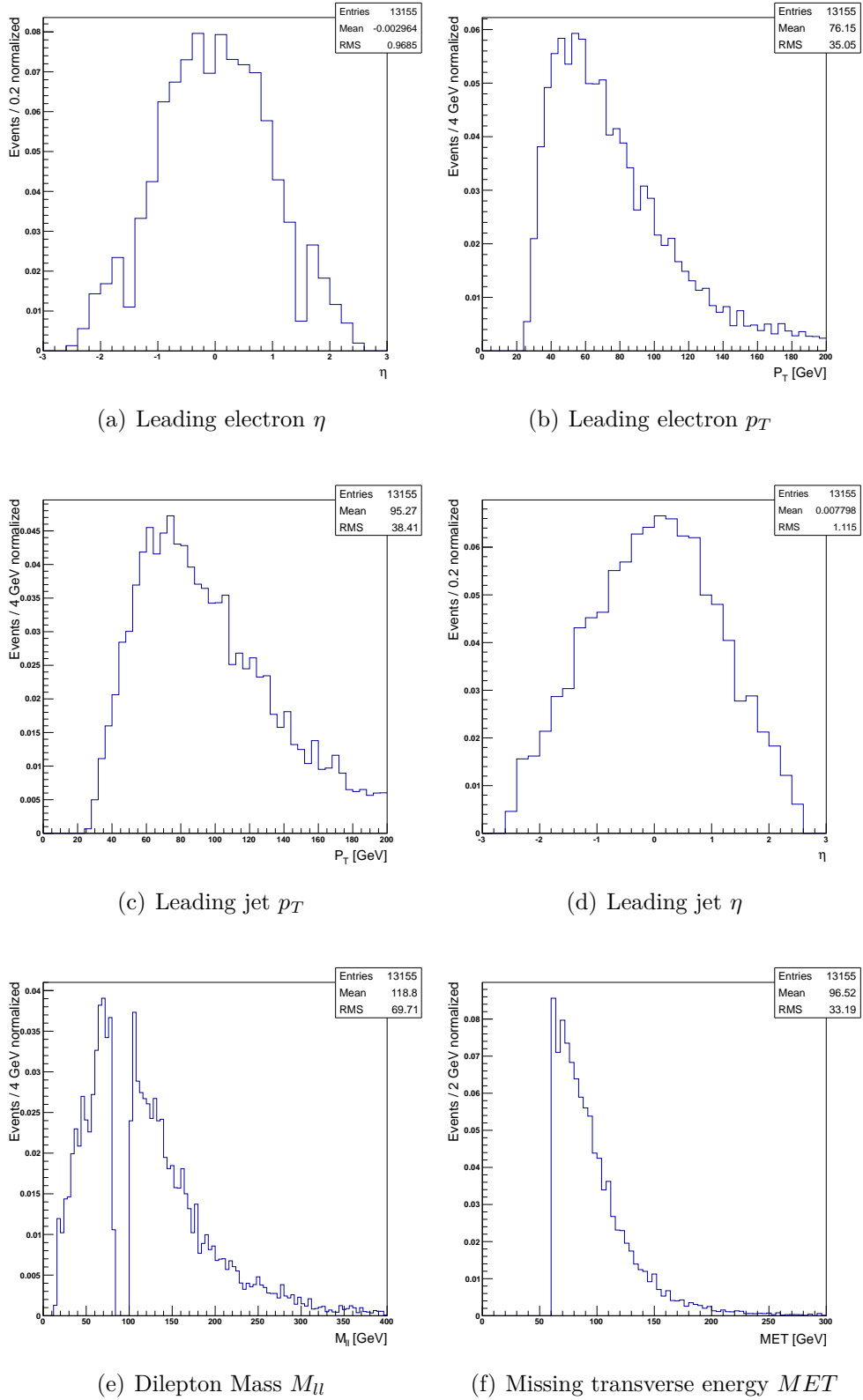
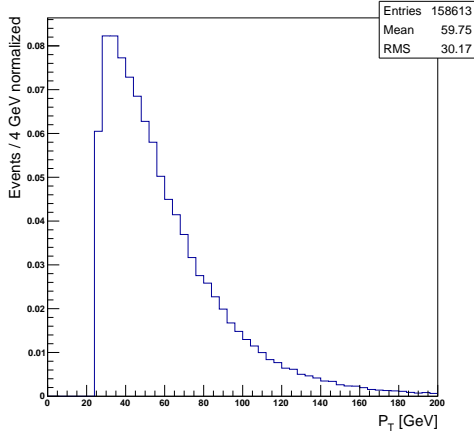
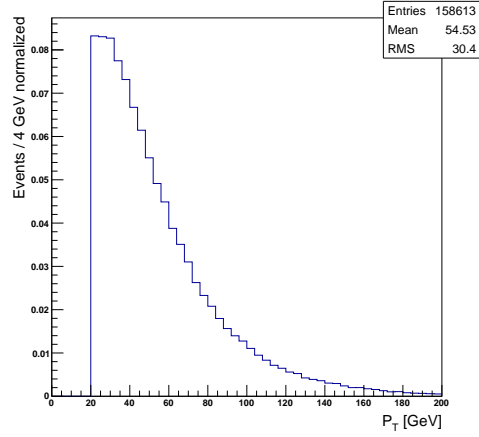
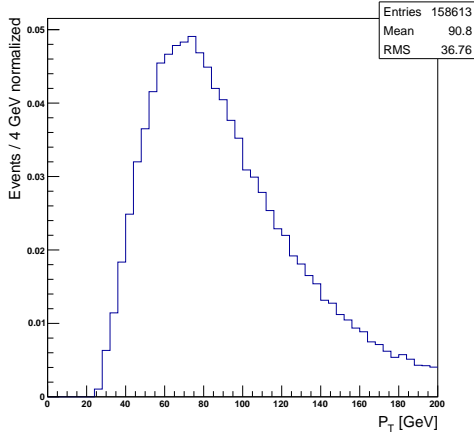
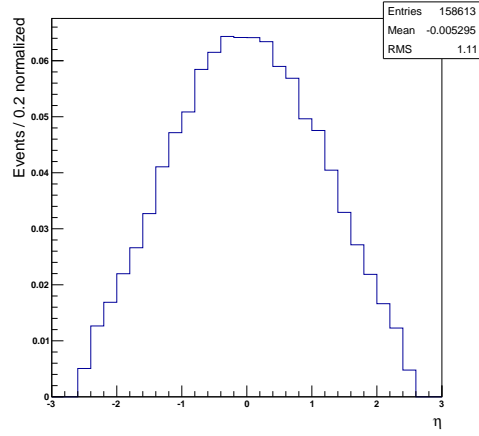
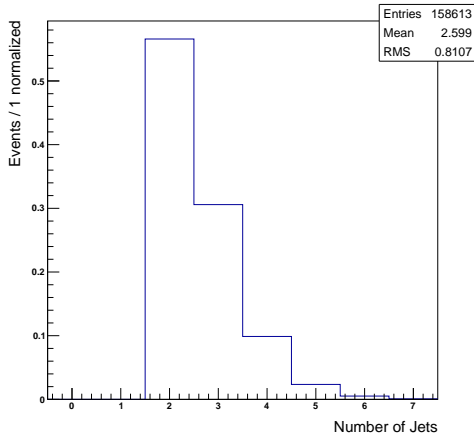


Figure 7.6.: Distributions of kinematic and topological distributions for $m_t = 172.5$ GeV in the ee channel after applying the event selection.

(a) Leading electron p_T (b) Leading muon p_T (c) Leading jet p_T (d) Leading jet η 

(e) Number of Jets

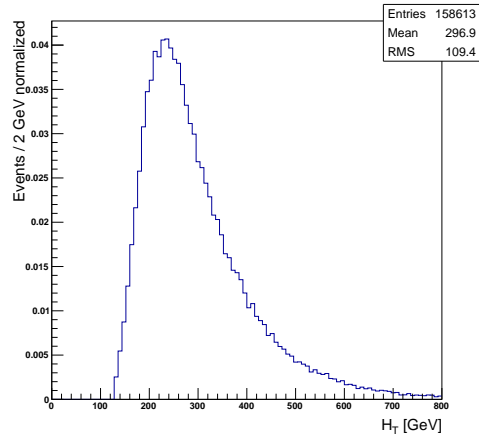
(f) Sum of transverse momenta H_T

Figure 7.7.: Distributions of kinematic and topological distributions for $m_t = 172.5$ GeV in the $e\mu$ channel after applying the event selection.

7.3.2. Gaussian fit to the Neutrino Pseudorapidity Distribution

In this section the differences for the Gaussian fit to the neutrino pseudorapidity distribution between parton and reconstruction level will be described. Figure 7.8(a) shows the Gaussian fit again for $m_t = 172.5$ GeV in the ee channel. In comparison

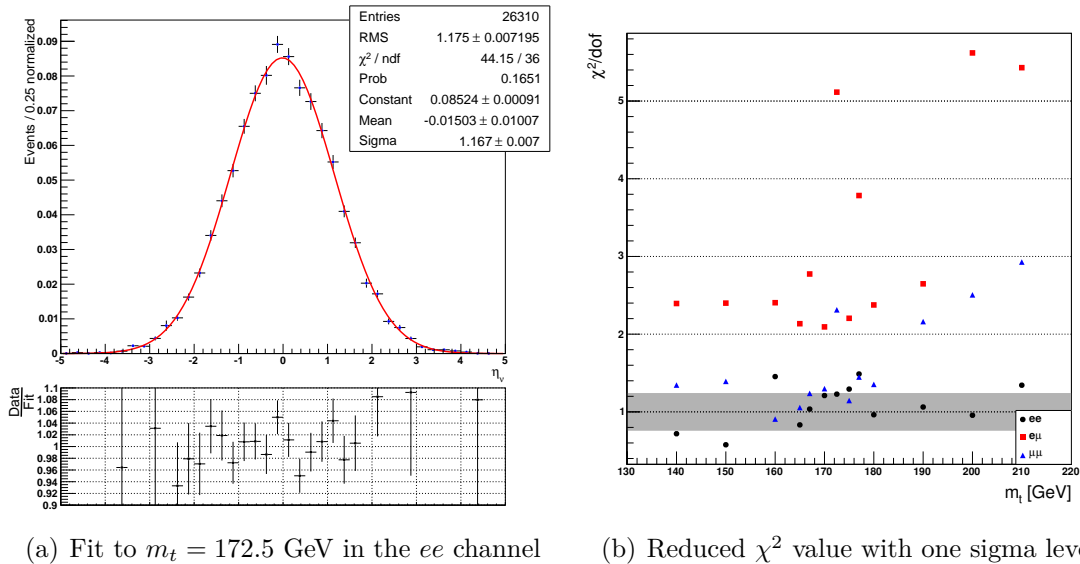


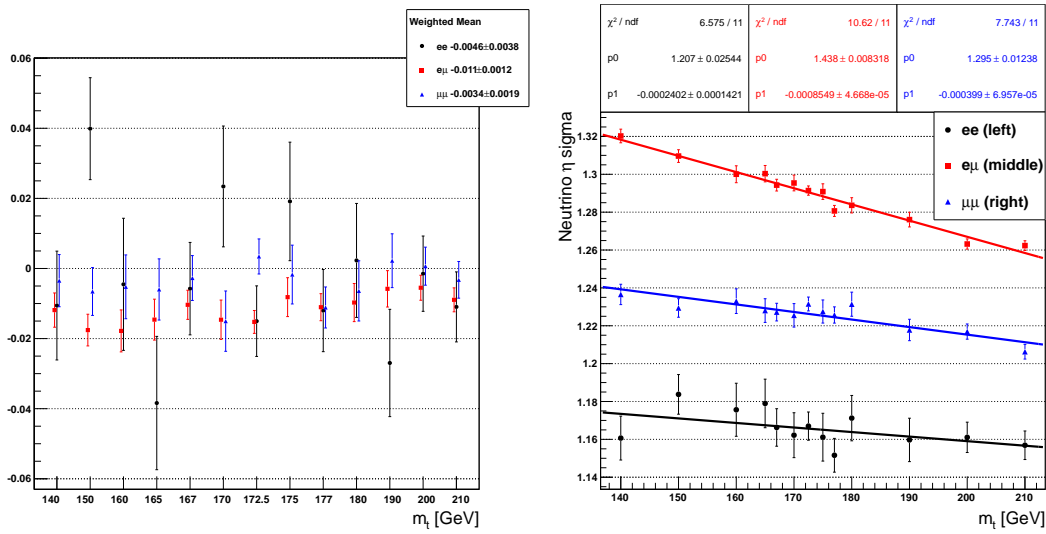
Figure 7.8.: Analysis of the Gaussian fit on reconstruction level

to the same histogram on reconstruction level, the number of entries on parton level (figure 7.3(a)) is almost 33 times larger. This leads to the increased statistical uncertainties per bin on reconstruction level and corresponds to reduced χ^2 values closer to one as can be seen in figure 7.8(b). The χ^2 values obtained from fits in the ee channel are close or within the one sigma level for the χ^2 distribution while the $e\mu$ values show the largest deviation to one. This is consistent with the different number of events in each channel (see table 7.1) and the χ^2 values on parton level (see figure 7.3(b)) which has a greater number of events overall. Thus, the pseudorapidity distribution in the ee channel can be better described by a Gaussian fit due to its larger uncertainties and not because the distribution actually has a Gaussian shape. The greater statistical uncertainties and the resulting fluctuations also hide the small systematic deviation in the ratio (figure 7.8(a), bottom) on reconstruction level which is caused by the neutrinos loosely following the top quark as discussed for the parton level.

7.3.3. The Parameter Dependence on the Top Mass

The constant C is given again by the normalization of the Gaussian. The mean value for each combination of top mass and channel is given in figure 7.9(a). Compared to the $\mu\mu$ and $e\mu$ channel, the fluctuations for the mean values in the ee channel are larger but can be explained by the smaller statistics in this channel. All shown values for the mean obtained from the Gaussian fit are again negligible compared to the width of the distribution and can be set to zero.

Figure 7.9(b) shows the dependence of the standard deviation on the top mass.



(a) Mean values for every channel and top mass (b) Fit to the standard deviation values using a first degree polynomial.

Figure 7.9.: Dependence on top mass of the parameters obtained by the Gaussian fit to the neutrino pseudorapidity distribution on reconstruction level.

The main difference to the parton level (figure 7.5(b)) is the split into the different channels. This difference is caused by the cuts applied in the event selection and will be discussed in the next section. In comparison to the parton level, the standard deviation is smaller for all top masses. Thus the event selection primarily removed events with larger neutrino pseudorapidities. A parameterization for the standard deviation is obtained by fitting a first degree polynomial. The results for ee (7.4),

7. Generator Studies

$e\mu$ (7.5) and $\mu\mu$ (7.6) are given below:

$$\sigma_{ee}(m_t) = (-2.40 \pm 1.42) \cdot 10^{-4} \cdot m_t [\text{GeV}] + (1.207 \pm 0.026) \quad (7.4)$$

$$\sigma_{e\mu}(m_t) = (-8.55 \pm 0.47) \cdot 10^{-4} \cdot m_t [\text{GeV}] + (1.438 \pm 0.009) \quad (7.5)$$

$$\sigma_{\mu\mu}(m_t) = (-4.00 \pm 0.70) \cdot 10^{-4} \cdot m_t [\text{GeV}] + (1.295 \pm 0.013) \quad (7.6)$$

The standard deviation in the ee channel has the smallest dependence on the top mass compared to the one in the $e\mu$ and $\mu\mu$ channel. Furthermore, the ee channel has the greatest uncertainty on the coefficients p_0 and p_1 which were obtained in the polynomial fit. This is again consistent with the lower overall statistics in this channel.

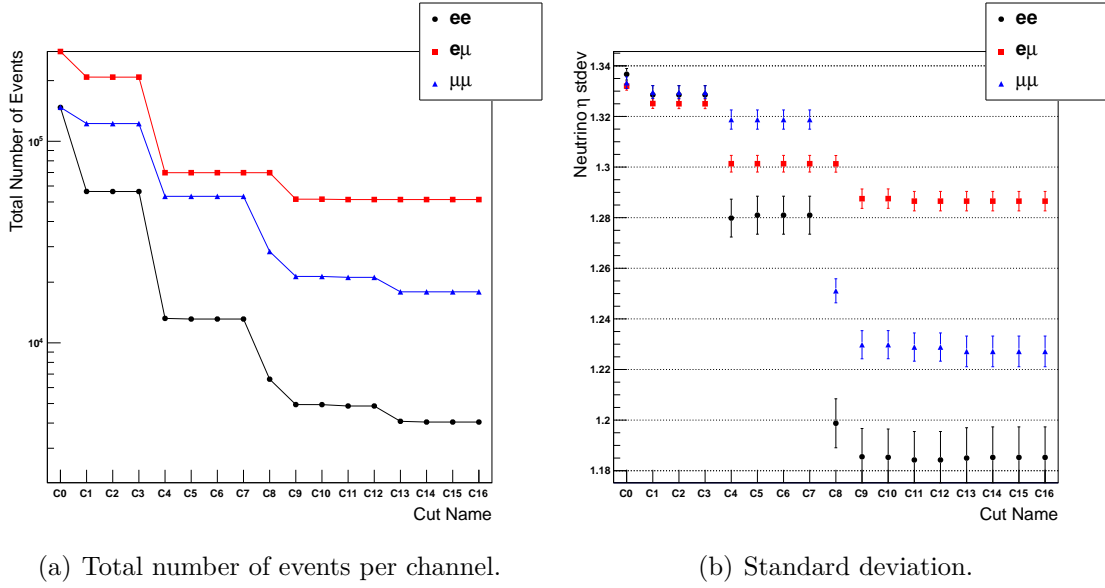
By integrating the Gaussian distribution (7.1) or by using an approximated expression for the error function one can now compute a variable number of steps in η which corresponds to the same number of events. This can be done for any top mass assumption due to the obtained parameterization and forms the pseudorapidity grid that is used to calculate the weight in the neutrino weighting algorithm.

Before the determination of the missing energy resolution a cutflow analysis is done in the next section to further investigate which selection criteria caused the distinct parameterizations for different channels.

7.3.4. Cutflow Analysis

In a cutflow analysis all cuts are added in succession and the impact on the results is studied. The cutflow analysis for $m_t = 165$ GeV is given in figure 7.10 and describes the development of the standard deviation and the total number of events while additional cuts are added in succession. While some selection criteria have almost no effect on those quantities there are some whose influence will be discussed in the following. All cuts are listed in appendix A. C0 is the previously discussed parton level while all cuts up to C16 combined correspond to the reconstruction level.

In C1 each event is required to be triggered which excludes a lot of events but shifts the standard deviation for each channel by approximately the same amount as can be seen in figure 7.10(b). The lepton selection, which determines the good leptons as described in 7.2, is applied in C4. The actual cut is the requirement of at least two of these good leptons. Each channel consists of different lepton flavours thus the impact of this cut is different for each channel and the values of the standard deviation split.



(a) Total number of events per channel.

(b) Standard deviation.

Figure 7.10.: Cutflow analysis for the $m_t = 165$ GeV sample. The cuts are given in appendix A. Cuts are applied in succession thus include all previous cuts.

C8 contains the cuts on the topological variables MET for the ee and $\mu\mu$ channel and H_T in case of the $e\mu$ channel. There are almost no events below the 130 GeV threshold for H_T , which is shown in 7.7(f). Therefore C8 cause no significant change in the $e\mu$ channel. The applied MET threshold excludes neutrinos with a small momentum in the transverse plane. At a fixed energy these neutrinos have a larger momentum in the z direction and therefore a larger η value. This results in a narrower neutrino pseudorapidity distribution and increases the difference of the $e\mu$ channel to the ee and $\mu\mu$ channel.

In C9 the good jets are determined and one requires at least two of them. This further reduces the standard deviation in all three channels. The last cut that removes a significant number of events is the application of the cut on the dilepton mass with respect to the mass of the Z^0 boson. However, this cut has almost no effect on the standard deviation.

The conclusion which can be drawn from this cutflow analysis is that the differences between the channels are due to the cuts on the lepton kinematic variables and the cut on the missing transverse energy. Furthermore, every single cut reduced the standard deviation thus one excludes primarily events with larger neutrino pseudorapidities.

7.3.5. The Missing Energy Resolution

The missing transverse energy resolution is determined by comparing the reconstructed missing transverse energy MET with the sum of the transverse momenta of both neutrinos based on their truth information. This is done separately for the x - and y -direction.

The weight (equation 5.4) assumes a Gaussian shape for this distribution. Therefore the missing energy resolution $\sigma_{\cancel{E}_{x/y}}$ is obtained via a Gaussian fit. The dis-

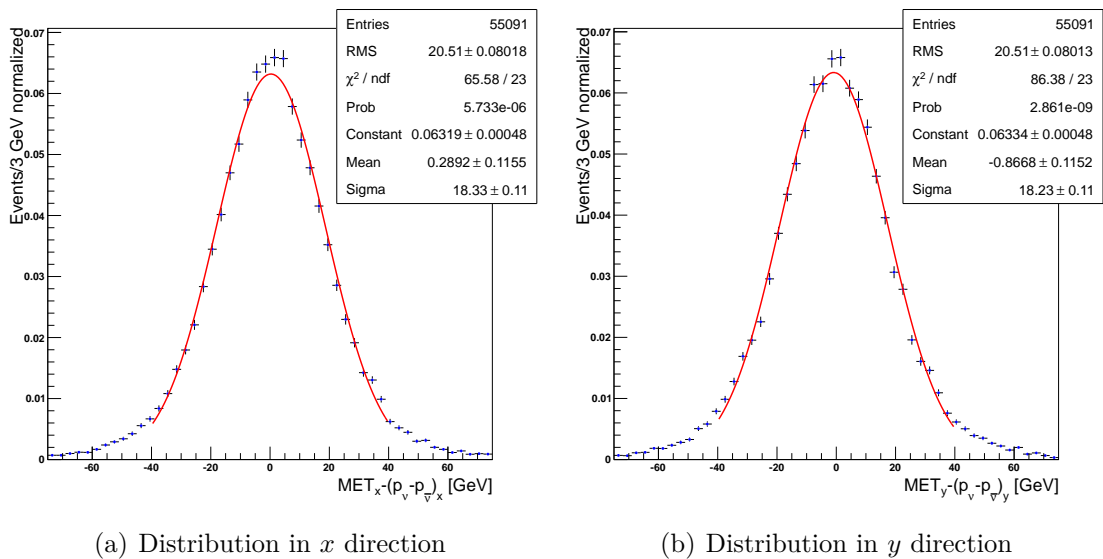


Figure 7.11.: Distributions for the difference between $MET_{x/y}$ and $(p_\nu + p_{\bar{\nu}})_{x/y}$ for $m_t = 172.5$ GeV in the $\mu\mu$ channel.

tributions for $m_t = 172.5$ GeV in the $\mu\mu$ channel are shown as an example in figure 7.11. The fit was constrained to $|MET_{x/y} - (p_\nu + p_{\bar{\nu}})_{x/y}| < 40$ GeV to better model the central region of the distribution. The obtained values for the mean of the Gaussian fit are small compared to its width so the most probable situation is $MET_{x/y} \approx (p_\nu + p_{\bar{\nu}})_{x/y}$. Therefore, there is no systematic discrepancy which is caused by unknown sources for missing energy and there is no offset that has to be included into the weighting formula.

The weight is calculated for different top mass assumptions so the dependence of the missing energy resolution on the top mass is studied in the following. The values for all different top mass and channel combinations are plotted in figure 7.12. The missing energy resolution increases for larger top masses in all channels and for

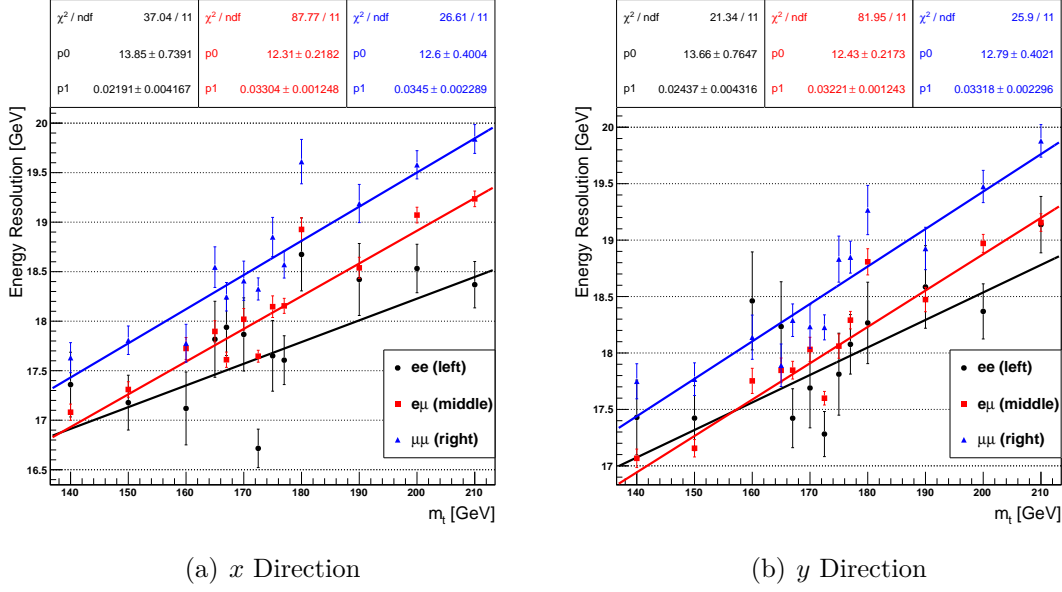


Figure 7.12.: Dependence of the missing energy resolution on the top mass for each channel described by a first degree polynomial fit.

both directions. Furthermore, there is no possible value that would be valid within the uncertainties for all top masses. The missing energy resolution depends on the uncertainties of MET measurements. The decay products of larger top masses have slightly larger transverse momenta. These momenta are calculated from the measurements of the track curvatures. Their relative uncertainty is proportional to p_T itself and thus the MET and its uncertainty are larger for larger top masses. This is consistent with the observation that the dependence on the top mass vanishes as soon as one repeats this analysis for a small MET interval.

The missing energy resolution has to be parameterized similar to the neutrino pseudorapidity standard deviation to be used in the neutrino weighting algorithm.

The first degree polynomial (equation 7.2) is used to obtain a parameterization for the missing energy resolution. The results of the fit in x -direction for the ee (7.7), $e\mu$ (7.8) and $\mu\mu$ (7.9) channel are given below:

$$\sigma_{\cancel{E}_x}^{ee}(m_t) = (2.19 \pm 0.42) \cdot 10^{-2} \cdot m_t + (13.85 \pm 0.74) \text{ GeV} \quad (7.7)$$

$$\sigma_{\cancel{E}_x}^{e\mu}(m_t) = (3.30 \pm 0.13) \cdot 10^{-2} \cdot m_t + (12.31 \pm 0.22) \text{ GeV} \quad (7.8)$$

$$\sigma_{\cancel{E}_x}^{\mu\mu}(m_t) = (3.45 \pm 0.23) \cdot 10^{-2} \cdot m_t + (12.60 \pm 0.40) \text{ GeV} \quad (7.9)$$

7. Generator Studies

The parameterizations in y -direction for the ee (7.10), $e\mu$ (7.11) and $\mu\mu$ (7.12) channel are computed to:

$$\sigma_{\cancel{E}_y}^{ee}(m_t) = (2.44 \pm 0.44) \cdot 10^{-2} \cdot m_t + (13.66 \pm 0.77) \text{ GeV} \quad (7.10)$$

$$\sigma_{\cancel{E}_y}^{e\mu}(m_t) = (3.22 \pm 0.13) \cdot 10^{-2} \cdot m_t + (12.43 \pm 0.22) \text{ GeV} \quad (7.11)$$

$$\sigma_{\cancel{E}_y}^{\mu\mu}(m_t) = (3.32 \pm 0.23) \cdot 10^{-2} \cdot m_t + (12.79 \pm 0.41) \text{ GeV} \quad (7.12)$$

Unlike the standard deviation of the neutrino pseudorapidity distribution the difference between the channels is not a result of the applied event selection. The electrons and muons are measured in different layers of the detector and thus have different uncertainties. Therefore, the uncertainties on the MET and the missing energy resolution depend on the channel.

The determination of the missing energy resolution concludes the preliminary studies that are needed in order to implement the neutrino weighting algorithm and to calculate a value for the top mass.

8. Conclusions and Outlook

In this bachelor thesis, dileptonic $t\bar{t}$ decays for 13 different top masses between 140 and 210 GeV generated by Monte Carlo simulations were studied. The focus of these studies was the dependence of the neutrino pseudorapidity on the top mass. Furthermore, the missing energy resolution was determined.

It was shown that the neutrino pseudorapidity distributions can be sufficiently well described by a Gaussian distribution at a center-of-mass energy of $\sqrt{s} = 7$ TeV. However, the studies on parton level revealed that the neutrino loosely follows the direction of the top quark it stems from. The pseudorapidity distribution shows indications that it has two peaks with respect to a Gaussian fit but the deviations are about 2% and can be neglected. It was described that one expects this effect to be larger for higher center-of-mass energies. Therefore, a Gaussian fit might not be sufficient when the LHC is updated to a higher center-of-mass energy because the deviation between the data and this fit would not be negligible anymore.

A parameterization for the standard deviation of this Gaussian fit to the neutrino pseudorapidity distribution was determined as a function of the top mass. This standard deviation decreases for increasing top masses, so the pseudorapidity distributions for larger top masses are narrower. On parton level, the standard deviation is the same for the ee , $e\mu$ and $\mu\mu$ channel. The results at reconstruction level, which are relevant for the next steps towards a top mass measurement, depend on the channel due to the event selection which has a different effect on each channel. Therefore one has to update the parameterizations as soon as the selection criteria are changed.

Additionally, the missing energy resolution $\sigma_{\cancel{E}}$ was studied on reconstruction level. Although this is a detector property, it was shown that a slight dependence on the top mass due to the uncertainty of the missing transverse momentum measurement has to be considered. Therefore, a parameterization was calculated for each channel and separately for the x - and y -direction.

As stated throughout chapter 7, all tests that were performed have been successful

8. *Conclusions and Outlook*

and their results were consistent with each other and the expectations. This concludes the preliminary studies that are needed to implement the neutrino weighting algorithm.

With the parameterizations for the standard deviation of the neutrino pseudorapidity given in section 7.3.3, a grid of neutrino pseudorapidities can now be calculated for any top mass assumption. A weight can be calculated for each top mass and for each event by comparing the calculated and observed missing transverse energy and using the parameterization for the missing energy resolution in section 7.3.5.

A. Full List of Cuts in Event Selection

Index	Description
C0	The event is a true dileptonic $t\bar{t}$ decay.
C1	It was triggered in the detector.
C2	One requires a primary vertex for the $t\bar{t}$ decay.
C3	A rejection for cosmic muons is applied.
C4	The event must have at least two good leptons.
C5	One of these leptons has to match the trigger.
C6	e and μ must not overlap in the event.
C7	Jets are required to be clean and MET tool for the liquid argon problem is applied.
C8	MET and H_T cuts are applied.
C9	There have to be at least two good jets.
C10	There are exactly two leptons.
C11	Both of these leptons must have opposite charges.
C12	Cut to the dilepton mass of $ m_{ll} - m_{Z^0} > 10$ GeV.
C13	The dilepton mass $m_{ll} = \sqrt{(p_{l_1} + p_{l_2})^2}$ must exceed 15 GeV.
C14	The two leptons have to match the true leptons from the $t\bar{t}$ decay.
C15	Number of b -tagged jets cut (currently not used).
C16	Cut on the liquid argon error flag.

B. Literature

- [1] PARTICLE DATA GROUP, *Particle Physics Booklet*. July 2010, (2010), IOP Publishing Geneva/Berkeley
- [2] WWW-ZEUS.DESY.DE, on page: *Alcune immagini sulla fisica elettrone-protone e l'esperimento ZEUS*, retrieved: 4.7.2012 at 9:48: http://www-zeus.desy.de/~bellagam/figure/desy/materiebausteine_en.jpg
- [3] S. WEINBERG, A Model of Leptons, (1967), *Physical Review Letters* Vol. 19 p. 1264
- [4] S. WEINBERG *et al.*, Electromagnetic and Weak Interactions, (1964), *Physical Letters* Vol. 13 p. 168
- [5] S. L. GLASHOW, Partial Symmetries of Weak Interactions, (1961), *Nuclear Physics* Vol. 22 p. 579
- [6] N. CABIBBO, Unitary Symmetry and Leptonic Decays, (1963), *Physical Review Letters* Vol. 10 p. 531
- [7] M. KOBAYASHI & T. MASKAWA, CP-Violation in the Renormalizable Theory of Weak Interaction, (1973), *Progress of Theoretical Physics* Vol. 49 p. 652
- [8] THE KAMIOKANDE COLLABORATION, Solar Neutrino Data Covering Solar Cycle 22, (1996), *Physical Review Letters* Vol. 77 N.9
- [9] THE SNO COLLABORATION, Direct Evidence for Neutrino Flavor Transformation from Neutral-Current Interactions in the Sudbury Neutrino Observatory, (2002), *Physical Review Letters* Vol. 89, 011301
- [10] R. DE PUTTER *et al.*, New Neutrino Mass Bounds from Sloan Digital Sky Survey III Data Release 8 Photometric Luminous Galaxies, (2012), arXiv:1201.1909
- [11] P. HIGGS, Broken Symmetries and the Masses of Gauge Bosons, (1964), *Physical Review Letters* Vol. 13 p. 508
- [12] F. ENGLERT & R. BROUT, Broken Symmetries and the Mass of Gauge Vector Bosons, (1964), *Physical Review Letters* Vol. 13 p. 321
- [13] THE ATLAS COLLABORATION, Observation of an Excess of Events in the Search for the Standard Model Higgs Boson with the ATLAS Detector at the LHC, (2012), ATLAS-CONF-2012-093
- [14] THE CMS COLLABORATION, Observation of a New Boson with a Mass near 125 GeV, (2012), CMS-PAS-HIG-12-020

B. Literature

- [15] THE ATLAS COLLABORATION, Observation of a New Particle in the Search for the Standard Model Higgs Boson with the ATLAS Detector at the LHC, (2012), Physical Letters B Vol. 716 p. 1-29
- [16] THE CMS COLLABORATION, Observation of a New Boson with a Mass near 125 GeV with the CMS Experiment at the LHC, (2012), Physical Letters B Vol. 716 p. 30-61
- [17] THE CDF COLLABORATION, Observation of Top Quark Production in $p\bar{p}$ Collisions with the Collider Detector at Fermilab, (1995), Physical Review Letters Vol. 74 p. 2626
- [18] THE D0 COLLABORATION, Observation of Top Quark, (1995), Physical Review Letters Vol. 74 p. 2632
- [19] K. NAKAMURA *et al.* (Particle Data Group), The Top Quark, (2010), JPG Vol. 37, 075021
- [20] A. QUADT, Top Quark Physics at Hadron Colliders, (2006), European Physical Journal C Vol. 48 p. 835
- [21] H.L. LAI *et al.*, New Parton Distributions for Collider Physics, (2010), Physical Review D Vol. 82, 074024
- [22] HEPDATA.CEDAR.AC.UK, on page: *Online PDF plotting and calculation*, retrieved: 3.7.2012 at 17:23: <http://hepdata.cedar.ac.uk/pdf/pdf3.html>
- [23] TWIKI.CERN.CH, on page: *ATLAS Experiment - Public Results*, retrieved: 6.7.2012 at 11:13: https://twiki.cern.ch/twiki/pub/AtlasPublic/CombinedSummaryPlots/TTBarXSec_may12.pdf
- [24] THE ATLAS COLLABORATION, Measurement of the Top Quark Charge in pp collisions at $\sqrt{s} = 7$ TeV in the ATLAS Experiment, (2011), ATLAS-CONF-2011-141
- [25] TEVATRON ELECTROWEAK WORKING GROUP, Combination of CDF and DO results on the mass of the top quark using up to 5.8 fb^{-1} of data, (2011), arXiv:1107.5255
- [26] A. KNUE, Measurement of the W helicity in top quark decays with the ATLAS detector using a template method, (2011), ATL-PHYS-PROC-2011-246
- [27] G. AAD *et al.*, Observation of Spin Correlation in $t\bar{t}$ Events from pp Collisions at $\sqrt{s} = 7$ TeV Using the ATLAS Detector, (2012), Physical Review Letters Vol. 108, 212001
- [28] THE ATLAS COLLABORATION, Measurement of the Charge Asymmetry in Top Quark Pair Production in pp collisions at $\sqrt{s} = 7$ TeV Using the ATLAS Detector, (2012), The European Physical Journal C Vol. 72, 2039
- [29] L. EVANS & P. BRYANT, LHC Machine, (2008), Journal of Instrumentation Vol. 3, S08003
- [30] TWIKI.CERN.CH, on page: *ATLAS Experiment - Public Results*, retrieved: 3.7.2012 at 17:29: <https://twiki.cern.ch/twiki/bin/view/AtlasPublic/LuminosityPublicResults>
- [31] THE ATLAS COLLABORATION, The ATLAS Experiment at the CERN Large Hadron Collider, (2008), Journal of Instrumentation Vol. 3, S08004

- [32] WWW.ATLAS.CH, on page: *ATLAS Experiment - Photos*, retrieved: 24.6.2012 at 12:18: http://www.atlas.ch/photos/atlas_photos/selected-photos/full-detector/0803012_01-A4-at-144-dpi.jpg
- [33] S. RAMO, Currents Induced by Electron Motion, (1939), Proceedings of the IRE Vol. 27 p. 584
- [34] JÖRG MEYER, *Measurement of the Top Quark Mass using Dilepton Events and a Neutrino Weighting Algorithm with the DØ Experiment at the Tevatron (Run II)*, Friedrich-Wilhelm-Universität Bonn, 2007, <http://hss.ulb.uni-bonn.de/2007/1277/1277.htm>
- [35] S. FRIXIONE AND B. R. WEBBER, Matching NLO QCD computations and parton shower simulations, (2002), Journal of High Energy Physics Vol. 0602, 029
- [36] G. CORCELLA *et al.*, HERWIG 6: an Event Generator for Hadron Emission Reactions with Interfering Gluons (including Supersymmetric Processes), (2002), Journal of High Energy Physics Vol. 0101, 010
- [37] J. M. BUTTERWORTH, J. R. FORSHAW, AND M. H. SEYMOUR, Multiparton Interactions in Photoproduction at HERA, (1996), Zeitschrift für Physik C Vol. 72 p. 637
- [38] S. AGOSTINELLI *et al.*, Geant4 A Simulation Toolkit, (2003), Nuclear Instruments and Methods A Vol. 506 p. 250
- [39] THE ATLAS COLLABORATION, The ATLAS Simulation Infrastructure, (2010), European Physical Journal C Vol. 70 p. 823
- [40] THE ATLAS COLLABORATION, Measurement of the Top Quark Pair Production Cross Section in pp Collisions at $\sqrt{s} = 7$ TeV in Dilepton Final States with ATLAS, (2011), ATLAS-CONF-2011-100
- [41] THE ATLAS COLLABORATION, Measurement of Spin Correlation in $t\bar{t}$ Production from pp Collisions at $\sqrt{s} = 7$ TeV using the ATLAS Detector, (2011), ATLAS-CONF-2011-117
- [42] M. CACCIARI, G. SALAM, G. SOYEZ, The anti- k_T jet clustering algorithm, (2008), Journal of High Energy Physics Vol. 4, 063
- [43] THE ATLAS COLLABORATION, Performance of the Missing Transverse Energy Reconstruction and Calibration in Proton-Proton Collisions at a Center-of-Mass Energy of $\sqrt{s} = 7$ TeV with the ATLAS Detector, (2010), ATLAS-CONF-2010-057

Acknowledgment

First of all I would like to thank Prof. Dr. Arnulf Quadt for giving me the opportunity to write my bachelor thesis in particle physics and for being the first referee of this thesis. Furthermore, my thanks go to Prof. Dr. Ariane Frey for being the second referee.

I wish to thank my supervisor Dr. Kevin Kroeninger for all the helpful discussions on top physics and for proof-reading this thesis. His ability to make the top physics clear to a beginner in particle physics is indispensable.

My sincere thanks go to Tamara Vazquez-Schröder. The tremendous effort and patience she invested in the supervision of my thesis cannot be appreciated enough. There has not been a single moment when she could not be bothered by questions. Thank you!

Moreover, I owe thanks to all the members of the institute, especially to the top working group, for all the fast and profound help as soon as there were any complications.

Erklärung nach §13(8) der Prüfungsordnung für den Bachelor-Studiengang Physik und den Master-Studiengang Physik an der Universität Göttingen:

Hiermit erkläre ich, dass ich diese Abschlussarbeit selbständig verfasst habe, keine anderen als die angegebenen Quellen und Hilfsmittel benutzt habe und alle Stellen, die wörtlich oder sinngemäß aus veröffentlichten Schriften entnommen wurden, als solche kenntlich gemacht habe.

Darüberhinaus erkläre ich, dass diese Abschlussarbeit nicht, auch nicht auszugsweise, im Rahmen einer nichtbestanden Prüfung an dieser oder einer anderen Hochschule eingereicht wurde.

Göttingen, den 6. November 2012

(Dominik Müller)